Characterization of ReNCell for studying chromatin associated proteins MeCP2 and histone H1

by

Bo Hyun “Cindy” Kim

B.Sc. with Hons. Biochemistry and Microbiology, University of Victoria, 2019

A Thesis Submitted in Partial Fulfillment of the Requirements for the Degree of

MASTER OF SCIENCE

In the Department of Biochemistry and Microbiology

Supervisory Committee

Supervisory Committee

Dr. Juan Ausió
Department of Biochemistry and Microbiology
Supervisor

Dr. Chris Nelson
Department of Biochemistry and Microbiology
Departmental Member

Dr. Kerry Delaney
Department of Biology
Outside Member

Abstract

Methyl-CpG binding protein 2 (MeCP2) and histone H1 are important chromatin associated proteins. Both exhibit their own extent of complexity as MeCP2 is an intrinsically disordered protein (IDP) that interacts with many different partners involved in several cellular processes and histone H1 consists of 11 different subtypes each of them associated with different posttranslational modifications (PTMs). An interesting avenue for the study of these proteins is in neurons where MeCP2 is very abundant and histone H1 level is half that observed in other somatic tissues. Several reports in the past have proposed that this lower level of histone H1 is due to the abundance of MeCP2 which displaces histone H1. However, this hypothesis has been debated and there is no clear consensus. In an attempt to study this controversy, a cell model system ReNCell WT and MeCP2-KO was used that can be induced to differentiate into neurons. The protein levels, transcript levels and localization of histone H1 subtypes in these cells were analyzed using HPLC, RT-qPCR and immunofluorescence, respectively. The results show that ReNCell WT and MeCP2-KO do not exhibit significant differences in their relative amount of histone H1 protein and transcript level neither at the proliferative nor at the later differentiated stages. However, HPLC analyses show that the histone H1 subtypes of these two cell types exhibit significant elution differences probably resulting from differences in their PTM content. Immunofluorescence analyses show that WT ReNCell differentiation as determined by extension of dendritic or axonic processes can be seen to occur over the course of one week and there is a significant difference in the nuclear area of these two cells at 8 DIV. This study provides important preliminary data for future research in MeCP2 and histone H1 using this cell model system and show that MeCP2 may have a bearing on histone H1 PTMs.

Table of Contents

List of Tables

List of Figures

List of Abbreviations

ACN	Acetonitrile
A230	Absorbance at 230 nm
ADP	Adenosine diphosphate
bFGF	Basic fibroblast growth factor
bp	Base pair
ChIP-Seq	Chromatin immunoprecipitation sequencing
CM	Chicken marker (chicken erythrocyte histones)
CNS	Central nervous system
CREB	cAMP response element-binding proteins
CTCF	CCCTC-binding factor
CTD	C-terminal domain
DAPI	4',6-diaminidino-2-phenylindole
DIV	Days *in vitro* (days after differentiation is induced)
DMEM	Dulbecco's modified Eagle medium
DNA	Deoxyribonucleic acid
DSB	Double-strand break
E14	Embryonic day 14
EGF	Epidermal growth factor
ESC	Embryonic stem cell
GAPDH	Glyceraldehyde-3-phosphate dehydrogenase
GD	Globular domain
Hi-C	High coverage chromatin conformation capture
HL	HeLa
HMG	High mobility group
HPLC	High-performance liquid chromatography
ID	Intervening domain
IDP	Intrinsically disordered protein
IF	Immunofluorescence
KO	Knockout (if used in the context of ReNCell, MeCP2-KO)
MBD	Methyl-CpG binding domain
MeCP2	Methyl-CpG binding protein 2
MS	Mass spectrometry
mu	Milliunits
NCoR	Nuclear receptor co-receptor
NCP	Nucleosome core particle
NPC	Neural progenitor cell
ncRNA	Non-coding RNA

NRL	Nucleosomal repeat length
NTD	N-terminal domain
P4	4 days after birth
PAGE	Polyacrylamide gel electrophoresis
PBS	Phosphate buffered saline
PCA	Perchloric acid
PFA	Paraformaldehyde
PTM	Posttranslational modification
RN	ReNCell (ReN cell)
RNA	Ribonucleic acid
RP-HPLC	Reverse phase high-performance liquid chromatography
RPLP0	Ribosomal protein lateral stalk subunit P0
RT-qPCR	Reverse transcription quantitative polymerase chain reaction
RTT	Rett syndrome
SDS	Sodium dodecyl sulfate
TAD	Topologically associating domain
TKO	Triple knockout
TRD	Transcription repression domain
VM	V-myc
WHD	Winged helix domain
WT	Wildtype (if used in the context of ReNCell, refers to intact MeCP2)

Acknowledgements

I have many people I would like to thank for helping me during this journey. Thank you, Juan, for giving me this opportunity to learn that science is vast and beautiful (and dealing with my many moments of panic). Important thanks also to Dr. Manel Esteller, Sonia Guil and Edilene Siqueira from the Josep Carreras Leukemia Research Institute of Barcelona, Barcelona, Catalonia, Spain for sharing with me the MeCP2-KO ReNCell line and providing guidance. Thanks to Nicoletta Landsberger and Angelissa Frasca from Italy for providing WT and KO mouse brains. This work was supported by a grant of the Ontario Rett Syndrome Association (ORSA) and by the Natural Science and Engineering Research Council of Canada (NSERC) Grant RGPIN-2017-04162. Thank you, Kat, Ladan and Jenna being the best lab mates that I could ever ask for. Thank you, Berna, Rachel, Ed, Noah, Baran, Ellis and Tian for your hangouts, encouragement, and ideas. Thank you, Kaleigh, Melinda and Kim, for helping me through administrative work. Thank you, Scott, Ryan and Steve, for your help and for fixing the many things I broke. Thank you, Drs. Delaney and Nelson, for your guidance and much help. Thank you, dad, grandparents and Judy, for your unending support. Thank you Wonjin for your love, support and protection. Thank you, Bella, for coming into my life at the most perfect time.

Chapter 1. Introduction

1.1 Chromatin and histone H1s

The fundamental unit of eukaryotic chromatin is the nucleosome which consists of about 200-bp DNA wrapped around an octamer of histone proteins[1]. The nucleosome core particle (NCP) is responsible for the wrapping of ~146 bp of DNA[2]. This octamer consists of two of each type of core histone, H2A, H2B, H3 and H4 (Fig. 1. 1). Core histones are important not only for packing and organizing the DNA but also for regulating gene expression with their vast array of variants and histone posttranslational modifications (PTM). Linker DNA is the segment of DNA where histone H1, the linker histone, can bind. Histone H1 can also bind the entry/exit point on the nucleosome close to the nucleosome dyad axis. When histone H1 binds to the nucleosome it constrains the DNA wrapping by an additional 20 bp beyond the NCP. The NCP-histone H1 complex is called the chromatosome[3]. Members of the histone H1 family are lysine-rich, positively charged proteins with three structural domains: an N-terminal domain (NTD) of 20-35 amino acids, a globular domain (GD) of ~70 amino acids and a longer C-terminal domain (CTD) of ~100 amino acids[4]. The globular domain is conserved between histone H1 subtypes and in different species, has a winged helix domain (WHD) which interacts with a region close to the NCP dyad axis while the more variable N- and C-terminal regions bind to the linker DNA[5]. There is an average of one histone H1 molecule per nucleosome in each mammalian cell[2] and therefore, histone H1 is a very abundant chromatin associated protein.

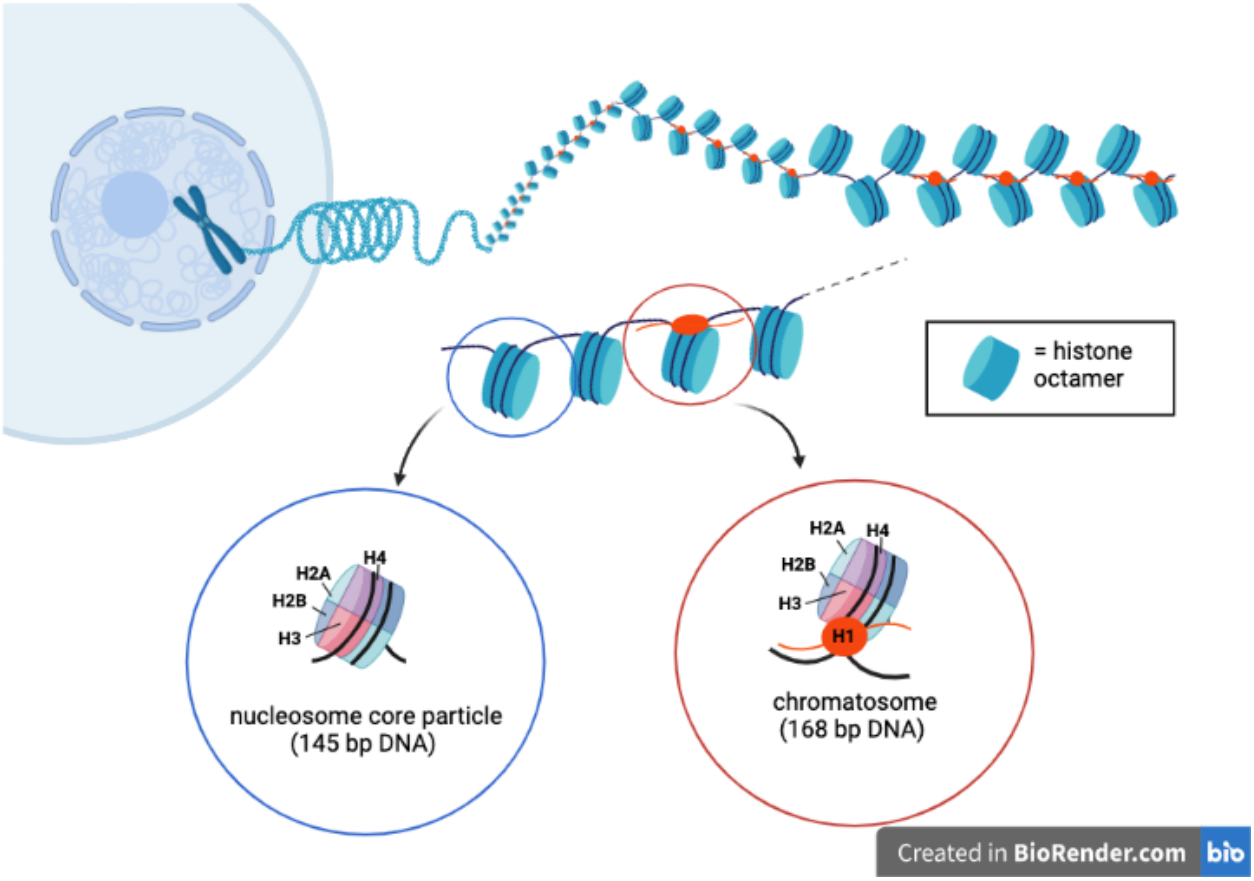

Figure 1. 1 Nucleosome core particle is the fundamental subunit of eukaryotic chromatin. DNA in the nucleus is wrapped around heterotypic histone octamer consisting of 2 copies of each of H2A, H2B, H3 and H4. The nucleoprotein complex consisting of 145bp DNA wrapped around a histone octamer is NCP. A nucleosome core particle plus a linker histone and the extra length of DNA bound by H1 is called a chromatosome. Chromatin is (the polynucleosome fiber) highly organized and linker histones are involved in maintaining the higher-order folding of chromatin. Image created in BioRender with the use of 'chromatin' template.

Histone H1 modulates the higher-order structural folding of the chromatin fiber. Histone H1 brings together the entry and exit regions of DNA around the nucleosome and in doing so, effects a more organized form of chromatin where nucleosomes adopt a zig-zag organization[6]. In *Drosophila*, histone H1 maintains the integrity of heterochromatin[7], a chromatin organization involved in maintaining gene silencing.

Because of their involvement in genome compaction, histone H1s were initially associated with gene silencing[8]. In *Drosophila*, H1 is depleted from transcription start sites of active genes where there is an enrichment of H3.3, a core histone variant associated with active genes[9]. When H3.3 is knocked down, H1 binds to these sites. However, this global effect observed in the fruit fly may not explain the full functionality of histone H1. Though mouse embryonic stem cells (ESCs) with three histone H1 subtypes knocked out and consequently half the level of normal histone H1s exhibit a less compacted chromatin organization[10], these cells did not display a drastic change in gene expression[10]. In fact, while some genes were downregulated as expected, other genes were upregulated with the deletion of histone H1s. These results speak to the complex involvement of histone H1s in different cell types and organisms. Despite this complexity, histone H1s are present in diverse organisms from very primitive protozoans and metazoans to humans, albeit at different stoichiometry with respect to the histone octamer (Table 1. 1). In *Saccharomyces cerevisiae*, there is a non-essential protein homolog similar to that of metazoan histone H1, encoded by the gene *HHO1*[11]. This protein has two globular domains as opposed to one in canonical histone H1. In *Tetrahymena,* histone H1s do not have the central globular domain[12]. In plants and animals, the winged-helix globular domain is conserved.

In mammals, there are as many as 11 different histone H1 subtypes: H1.1, H1.2, H1.3, H1.4, H1.5, H1.0, H1.x, H1t, H1T2, HILS and H1oo, the first seven of which correspond to the somatic subtypes and the last four, germline-specific subtypes. H1t, H1TS and HILS are testis-specific subtypes and H1oo is an oocyte-specific subtype. Among the somatic subtypes, H1.0 is a differentiation-specific H1 which increases with differentiation and development[13,14]. Because H1.0 is very distinct from other H1s and therefore the most immunogenic, many studies choose the H1.0 subtype for studying the histone H1 family. However, H1.0 is an atypical H1 as it is

shorter than the other somatic subtypes and while other vertebrate H1 subtypes are encoded on the same chromosome in the histone gene cluster, histone H1.0 is located on a completely different chromosome. In humans, the histone gene cluster is on chromosome 6 while H1.0 is on chromosome 22. In mouse, the histone gene cluster is on chromosome 13 while H1.0 is on chromosome 15. H1.0 is also replication-independent and hence it is expressed as a poly-adenylated mRNA while H1.1-H1.5 are replication-dependent, and their mRNAs are not poly-adenylated. This already indicates that H1.0 is differently regulated, and the results obtained with histone H1.0 do not necessarily reflect those that could be obtained from other H1 subtypes.

Because of the structural similarities between the somatic subtypes, it has often been assumed that they have redundant functions. A report used to support this hypothesis is Fan *et al*., (2001) where they showed that when one or even two histone H1 subtypes were knocked out in mouse ESCs, the other histone H1 subtypes increased in abundance to compensate for this loss and there was no noticeable functional change to the cells. However, it was subsequently shown that certain combinations of H1 subtype deletions led to compensation by the remaining H1 subtypes while others led to lethality. In mouse, when three different histone H1 subtypes (H1.2, 3 and 4) are knocked out so that only half the normal level of histone H1 is expressed, such deletions result in embryonic lethality[15]. Though the somatic histone H1 subtypes have similar primary sequence (Fig. 1. 2) and the early results suggested that there is some extent of functional redundancy, there is an increasing number of recent reports describing subtype-specific characteristics and functions. Because much of the variation amongst histone H1 subtypes is within the C-terminal domain which contributes most to the protein's affinity to DNA, each subtype has different binding affinities to chromatin; H1.3, H1.4 and H1.0 have the highest affinity for DNA whereas H1.1 has the lowest binding affinity[16].

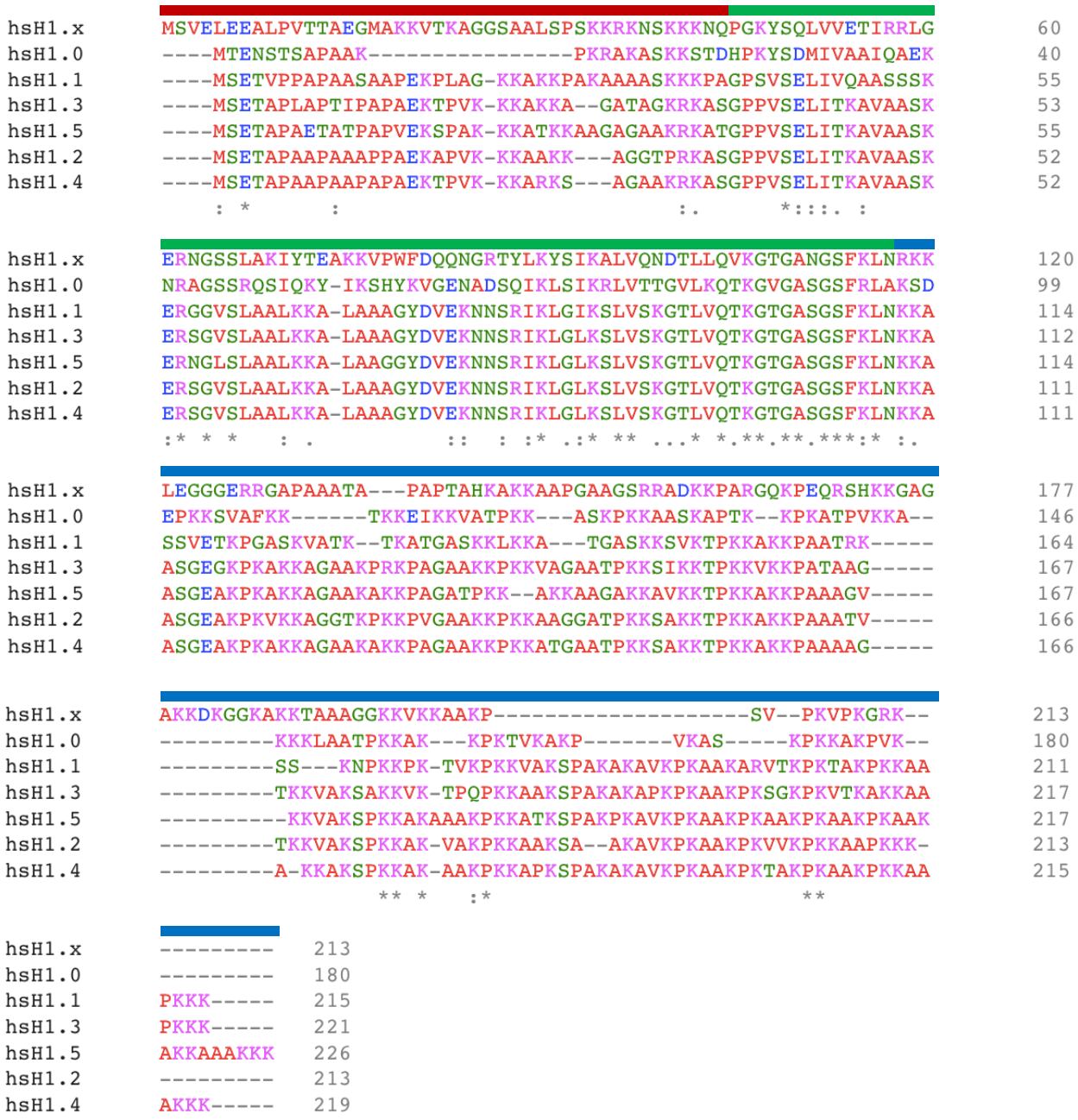

Figure 1. 2 Clustal Omega Multiple sequence alignment of human somatic histone H1 subtypes. Conserved residues shown with asterisks and colons below each row (asterisk; a single, fully conserved residue. Colon; conservation between groups of strongly similar properties). Domains of histone H1 are shown above each row as colored bars: red = NTD, green = GD, blue = CTD. For the colors of amino acid letters, red = small hydrophobic, blue = acidic, magenta = basic, green = hydroxyl, sulfhydryl, amine and glycine.

The studies carried out from the 1990s to today show that the expression levels of histone H1 subtypes appear to be tissue and cell-type specific. Some subtypes have been associated with specific functions, and in certain cases, have even been shown to be disease markers. In ovarian cancer, H1.3 is responsible for repressing the expression of a ncRNA and inhibiting cancer growth[17]. The KO of H1.4 in T47D cells (human breast cancer cell line) killed these cells[18]. In many cell lines examined, H1.2 and H1.4 are always present while the other somatic subtypes may be missing[19]. Histone H1.2 has been shown to be an effective antimicrobial agent against some burn wound infection pathogens[20]. Histone H1.2 also regulates DSB-induced apoptosis[21]. Histone H1.5 is suggested to be a biomarker of the prognosis of pulmonary neuroendocrine tumours[22] and prostate cancer[23]. These publications are accumulating evidence that each subtype has a non-redundant and specific function in certain contexts.

1.2 Histone H1 Posttranslational Modification (PTM)

Histone H1 function in chromatin is more nuanced as there is a plethora of PTMs that can affect linker histones. Compared to the PTMs of core histones, PTMs of linker histones are understudied. The most extensively studied and well-characterized PTM is that of cell-cycle dependent phosphorylation. Phosphorylation of histone H1 increases along the cell cycle, reaching a maximum during mitosis[24]. In fact, when histone H1 phosphorylation is inhibited by staurosporine (inhibitor of kinases that phosphorylate H1), chromatin decondenses and entry into mitosis is halted[25]. Though phosphorylation is the most studied PTM for linker histones, there are many other PTMs on H1s that have been described through the use of mass spectrometry techniques such as methylation, acetylation, formylation, propionylation, crotonylation, ADP-ribosylation, citrullination and others[26,27]. The diversity in histone H1 subtypes in combination

with PTMs make the protein very complex and its function difficult to understand. Further investigation is needed to get a good insight into the significance of linker histone PTMs.

1.3 MeCP2

Methyl-CpG binding protein 2 (MeCP2) is another important chromatin associated protein. MeCP2 was first characterized in 1992 by the Adrian Bird lab in a search for methyl-binding proteins[28]. MeCP2 is an intrinsically disordered protein (IDP). IDPs are disordered proteins that can adopt a secondary structure upon interacting with a partner[29]. Despite its IDP nature, MeCP2 has well-defined and distinct domains (Fig. 1. 3): methyl-CpG binding domain (MBD), ID (intervening domain), TRD (transcription repression domain) and CTD (C-terminal domain). The MBD mediates the binding to methylated DNA. The TRD has a well-known mechanism of gene transcription repression which is mediated by its association with NCoR-complex, a complex involved in gene repression mediated by histone deacetylases. Nucleosomes with methylated DNA promote MeCP2 to bind as a dimer while the protein binds to unmethylated nucleosomes as a monomer[30]. Despite an extensive characterization of the protein, many of its functions remain enigmatic. Part of this might be due to MeCP2 having varied functionality that is context-dependent.

Figure 1. 3 MeCP2 structural domains with amino acid numbers shown. Numbers correspond to the E2 isoform. Adapted from Ausió, de Paz and Esteller (2014)

Despite the protein's distinctive 'methyl-CpG binding' name, the CTD of the protein can also bind to unmethylated DNA and to some extent, the MBD also does albeit at a lower affinity than to methylated DNA[30,31]. MeCP2 has many positive residues and a pI of 9.9 which could confer its ability to bind to negatively charged DNA, regardless of its methylation status. Also, despite its TRD, MeCP2 has been shown to be able to activate some genes, a process mediated by its interaction with CREB specifically in the hypothalamus[32]. MeCP2 was also shown to be an RNA-binding protein[33]. The recently described RNA-binding function of MeCP2 may provide an explanation for some of the protein's unaccounted functions.

MeCP2 is expressed abundantly in neurons where its abundance increases during neuronal development[34,35]. Mutations in MeCP2 have been shown to be at the root of Rett syndrome (RTT)[36], a neurodevelopmental disorder that occurs in 1:10,000 live female births. Because MeCP2 is encoded on the X-chromosome, males who are hemizygous often die in utero or exhibit severe phenotype. Since the discovery of this correlation, many studies have been carried out on MeCP2 to try to elucidate the molecular mechanisms of the pathology. A child with Rett Syndrome develops seemingly normally until 6-18 months of age but afterwards, does not reach the normal developmental milestones. Children with RTT exhibit partial or complete loss of normal movement, partial or complete loss of verbal communication, hand stereotypies, breathing problems and loss of other cognitive abilities[37].

In neurons, MeCP2 has been shown to be involved in later stages of neuronal development such as maturation, maintenance and dendritic arborization[38]. Many studies on MeCP2 have shown its relevance to the differentiated state of neurons as compared to the neural progenitor stages. This appears to correspond well with the RTT phenotype where the child with mutations in MeCP2 does not exhibit any neurological symptoms until 6-18 months of age which

is a time of neuronal development. However, recent reports show that MeCP2 has some roles in triggering the differentiation of a neural stem cell into a progenitor cell[39]. Also, Singleton *et al*. (2011) suggested that the seemingly normal phenotype at early stages of life of RTT patients or in animal models hide the subnuclear malfunctions, such as improper rearrangement of chromocenters in the nucleolus[40]. Therefore, it is highly likely that MeCP2 is important for all stages of neuronal development. That MeCP2's functionality has the greatest implications in the brain is shown with MeCP2's association with many neurodevelopmental and neurodegenerative disorders besides Rett Syndrome: autism[41], schizophrenia[42], Huntington's[43], Parkinson's[44], depression[45] and fetal alcohol syndrome[46]. Hence, most of MeCP2 characterization to date has been performed in neurons because of its involvement in neurological disorders, its high levels of expression in neurons and partly because of the availability of mouse KO and reduced function mutants that mimic the RTT phenotype[47,48]. Nevertheless, because of the characteristic binding of MeCP2 to methylated DNA and as DNA methylation is a ubiquitous and highly important epigenetic mark, studies on the regulation of MeCP2 is pertinent to every tissue.

1.4 Histone H1 in neurons and the potential involvement of MeCP2 in histone H1 displacement

In cortical neurons, there is a decrease of the nucleosomal repeat length (NRL) right after birth[49] (Fig. 1. 6A). This is possibly due to the decrease in the molar abundance of histone H1 proteins which occurs at the same time as the NRL decrease. A study done with rat neurons showed that there is a significant drop in H1 abundance from embryonic day 16 (E16) to postnatal day 10 (P10)[50]. In these neurons, the overall level of histone H1 is half of that observed in other types of cells such as glia. While glia contain about one H1 molecule per nucleosome, in

neurons, there is only 0.45 H1 per nucleosome[51]. The reason for the decrease in histone H1 is currently unknown. One possible cause for this decrease could be the increase of MeCP2 along development, in particular that which occurs with the postnatal increase of methyl CH[52] (H = A, T, C). When MeCP2 is knocked out in the MeCP2-KO model, cortical neurons have twice the level of histone H1 as in neurons from a wild type mouse[53]. This suggests that MeCP2 acts as a partial linker histone replacement in neurons. In 1997, Adrian Bird's lab performed an elegant *in vitro* experiment that showed that MeCP2 was able to physically displace histone H1 in a DNA-methylation dependent manner[54] which suggests that MeCP2 has a higher affinity for methylated DNA than histone H1 (Fig. 1. 4). Ghosh *et al*. (2010) obtained similar results showing that MeCP2 and histone H1 compete for similar chromatin binding sites[30]. A mechanism proposed from these results is that as the level of MeCP2 rises during neuronal development, MeCP2 binds to regions that are normally occupied by histone H1, in the DNA regions where MeCP2 has higher affinity. Consequently, histone H1s would be displaced and degraded, resulting in the halved level of histone H1 observed in neurons.

However, the Zoghbi group recently has produced some conflicting results showing that the binding of MeCP2 and histone H1 is independent; that is, MeCP2 does not displace histone H1[55]. One issue with most of these papers though is that the histone H1 subtype used has systematically been histone H1.0. As mentioned earlier, histone H1.0 is a very specific subtype that is differently regulated compared to other somatic subtypes. Most notably, H1.0 accumulates in terminally differentiated cells[14]. As shown by Figure 1. 6B, H1.0 increases postnatally at around P15 at a time both the NRL transition and the histone H1 decrease have already taken place (Fig. 1. 6). Therefore, the relationship between histone H1.0 and MeCP2

Table 1. 1 Review of the linker histone/octamer ratios in different organisms and tissues. Adapted from van Holde (1989)[2]

Organism	Tissue/Cell	moles of linker histone/octamer	Reference
Chicken	Adult erythrocytes	2.32	Urban *et al*. (1980)
		2.4	Olins *et al*. (1976)
		1.3	Bates and Thomas (1981)
Ox	Glia	1.07	Bates and Thomas (1981)
Ox	Glia (Cerebral Cortex)	1	Pearson *et al*. (1984)
Ox	Neuron (Cerebral Cortex)	0.45	Pearson *et al*. (1984)
Mouse	Liver	0.74	Bates and Thomas (1981)
Mouse	ESC with TKO of histone H1s	50% of normal amount	Fan *et al*. (2003)
Mouse	MeCP2-KO neurons	Twice as much as WT neurons	Skene *et al*. (2010)

may not be representative of that taking place with other H1 subtypes. In this regard any other somatic subtypes would be a better choice for the analysis of the relationship between MeCP2 and histone H1 with histone H1.4 being one of the best candidates as it is the most abundant somatic histone H1 subtype.

Chromatin is a highly dynamic system with many chromatin associated proteins in constant binding flux. The regulation of these dynamics is important for proper functioning of cells. Though MeCP2 and histone H1 are both prominent chromatin associated proteins especially in neurons, there is still much unknown about their individual roles. Studying these proteins in combination can provide more insight into the mechanisms involved in the unique organization of neuronal chromatin.

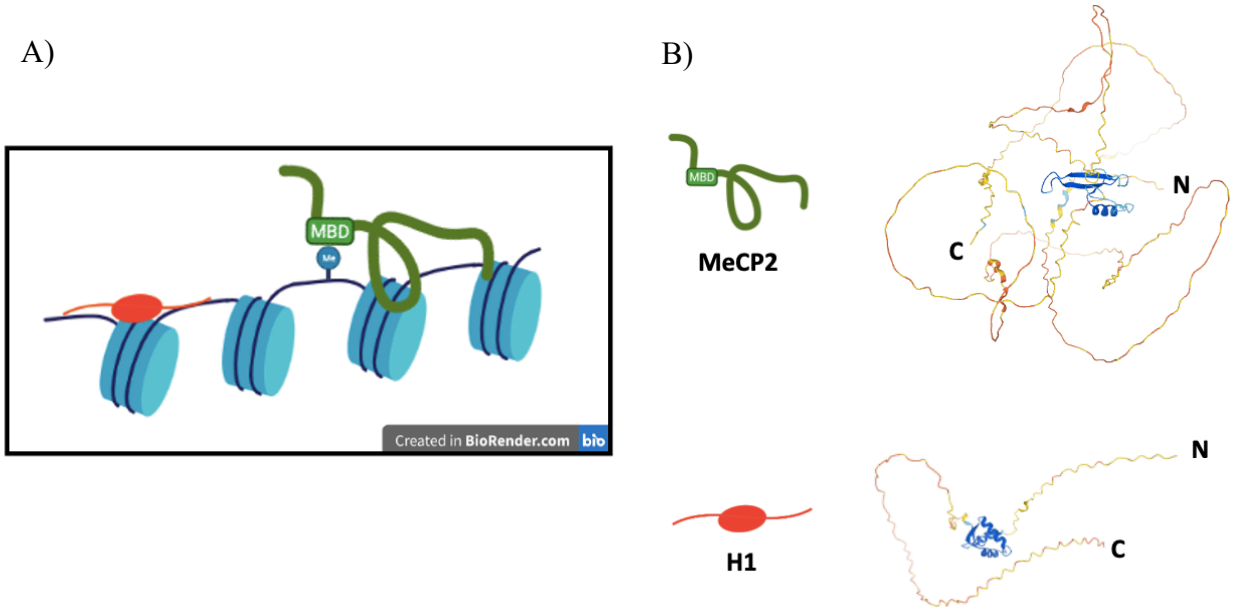

Figure 1. 4 A model of MeCP2 and histone H1 binding to nucleosomes A) A model to show how MeCP2 and histone H1 bind to nucleosomes. **B)** Alphafold structure predictions for MeCP2 and histone H1.4. N- and C-terminus of each protein are shown.

1.5 Visualization of the nuclear chromatin organization and cell differentiation

Regardless of the histone H1 composition of cortical neurons and its relatedness or not to its coexistence with MeCP2, alterations in the nuclear size during differentiation was observed in cortical neurons lacking MeCP2[40]. Similarly, a decrease in nuclear size was detected in cortical neurons expressing a MeCP2 mutant truncated at its NTD with an impaired MBD[56]. Although such changes have been attributed to the low levels of histone H1 which are anti-correlated with the MeCP2 presence in these neuronal cells[57], a clear explanation for these observations appears to be elusive. Indeed the nuclear changes observed in cortical neurons take place at differentiation times[40] at which the MeCP2 and histone composition of these cells are not any longer significantly affected (Fig. 1. 6).

While the presence or absence of histone H1 has been shown to play a role in the modulation of the nuclear size[58], many other factors may be involved in the establishment of the nuclear shape and conformation[59], such as for instance lamin B1 during corticogenesis[60].

The eukaryotic genome is compartmentalized within the nucleus in a three dimensional organization which has direct implications on functional chromatin processes such as gene expression, DNA repair and DNA replication. One level of genome organization is the distinction of the A/B compartment where A is generally the gene-rich, open and accessible region (euchromatin) and B is the gene-poor, closed and inaccessible region (heterochromatin). The A compartment is more frequently found near the center of the nucleus and the B compartment is near the periphery of the nucleus, often attached to the nuclear lamina (Fig. 1. 5A). Another tier of higher-order chromatin organization is the arrangement into topologically associated domains (TADs). TADs are regions of the chromosome which make spatial associations internally more frequently than with other regions of the genome (Dixon at al., 2012). The organization and distinctions of TADs are mediated by CCCTC-binding factor (CTCF) and cohesin proteins (Fig. 1. 5C). Hi-C (High-coverage Chromatin Conformation Capture) is a genome analysis technique[61] that allows for the depiction of TADs within a chromosome (Fig. 1. 5B). Hi-C data show that A compartment interact with A compartments and B with other B compartments. A closer look at Hi-C data show that there are instances of strong interaction (shown in dark red in the TAD triangle) where a gene regulatory element interacts with a gene within the same compartment (Fig. 1. 5D).

Due to the involvement of histone H1 in genome compaction and higher-order chromatin structure, the histone H1 subtypes are not unsurprisingly associated with TADs. Recent Hi-C results from Serna-Pujol et al (2022) showed that in their histone H1 TKO mouse ESC model,

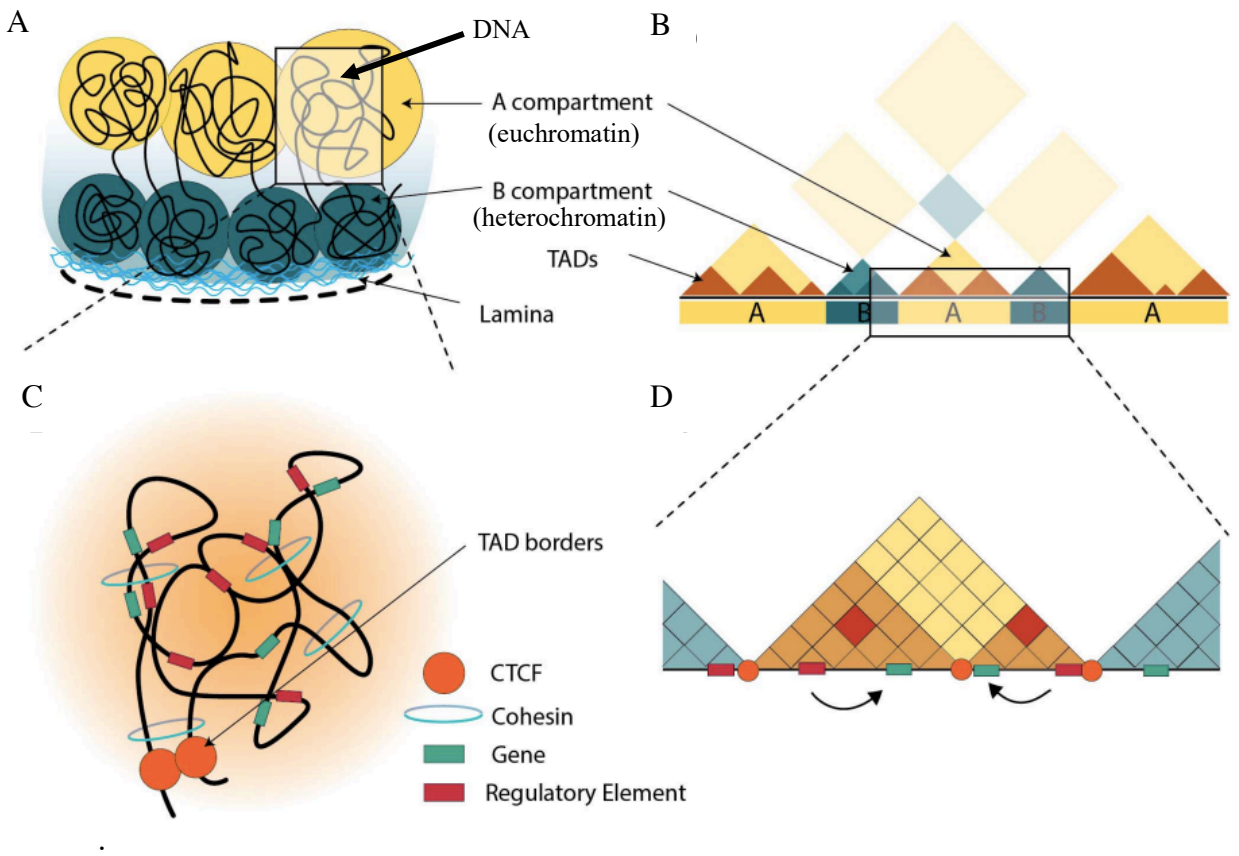

Figure 1. 5 Three dimensional organization of chromatin. A) Depiction of the arrangement of the A and B chromatin compartments within the nucleus. **B)** Hi-C data showing the interaction of the A compartment with another A compartment and B compartment with another B compartment. Topologically associated domains (TADs) are shown as interaction-rich triangles. **C)** DNA looping within one compartment is mediated by CTCF and Cohesin proteins. **D)** A close up of one compartment in the Hi-C data shown in B. Darker colors in the TAD triangles indicate regions of strong interaction (Adapted from Boltsis et al. (2021)[62]).

the existing TADs interacted more strongly within each TAD compared to the WT counterpart, resulting in a bolder distinction of individual TADs[63]. Moreover, histone H1 TKO resulted in more decompaction of TADs. Hi-C analysis of $CD8^+$ T cell with histone H1 TKO showed that some TADs within the B compartment switched to the A compartment due to the genome-wide decompaction caused by the low level of histone H1s. Therefore, the regulation of histone H1 proteins has implications for the proper three dimensional organization of the genome.

Despite the molecular detail organization of chromatin provided by Hi-C technique, a more coarse organization of chromatin within the nucleus can also be obtained by immunofluorescence (IF) and confocal microscope[64]. IF methods can be used also to visualize neural differentiation by the visualization of the distinct dendrite features, changes in cell morphology and protein differential localization in the nucleus. During neuronal differentiation, there are several changes such as a change in the size of nucleus and genome organization. One example of such change is that during the differentiation of ESCs into NPCs and then to neurons, though the boundaries of TADs remain the same for the most part, the interactions between TADs change[65]. Another example is the general openness of chromatin of stem cells[66].

In this study, ReNCell was used as a neuronal model to study histone H1 and MeCP2 dynamics in chromatin. ReNCell VM is a human neural progenitor cell line that can be triggered to differentiate into neurons, and it was developed by the ReNeuron company in the UK. The cell line was derived from the ventral mesencephalon of a male human fetus. Importantly, one of our collaborators in Spain from the Manel Esteller lab in Barcelona made an MeCP2-KO of this cell line and kindly shared these cells with us. These WT and MeCP2-KO ReN cells were used in this study to elucidate the dynamics of MeCP2 and histone H1 in the chromatin.

A very preliminary proteomic characterization of the ReN cell line has already been published including some IF images of these cells[67]. Hence, IF also provides an invaluable tool for monitoring the changes in cell morphology undergone by both the WT and KO ReN cells at the different DIVs (days *in vitro*: number of days after differentiation is initiated) studied in the present work.

1.6 Rationale for the models used in this study

Previous results from Adrian Bird's lab suggested that MeCP2 abundance in neurons results in the displacement of histone H1 which is responsible for the decreased levels of H1 in these cells[53]. However, in terms of chromatin localization, it seems that MeCP2 and H1 (or at least, H1.0) do not compete for DNA binding sites[68]. Therefore, whether MeCP2 has a significant bearing on the low levels of H1 in chromatin in cortical neurons is not well elucidated.

To avoid the potential inconsistencies introduced by the cell heterogeneity of different regions of the brain, in this study, ReNCell VM, a human neural progenitor cell line developed by Millipore that can be triggered to differentiate into neurons has been used along with its MeCP2-KO counterpart. Therefore, ReNCell could be used for studying the relationship between MeCP2 and histone H1 in a neuronal context.

For the work on histone H1, focus was put on one particular histone H1 subtype (H1.4) as there is an increasing number of reports being published which shed light on the subtype-specific functionality of these proteins and histone H1.4 is the most abundant subtype in neurons.

The initial work for this project was to analyze the levels of H1.4 in WT and MeCP2-KO ReNCell via quantitative westerns to ascertain whether the levels of H1.4 are higher when MeCP2 is knocked out and then, if that is the case, perform ChIP-Seq for H1.4 in the two cell lines in order to determine where the additional H1.4 are binding in the KO cell genome. Unfortunately, as the results section shows, the H1.4 antibody was not very reliable for quantitative purposes. Histone H1 subtype-specific antibodies tend to be unspecific because of the sequence similarities (Fig. 1. 2). Therefore, I switched directions to characterize ReNCell for further studies in the context of MeCP2 and histone H1. I acid-extracted histones from ReNCell

and separated histones using RP-HPLC. Using the chromatograms from HPLC, I calculated the ratio of total histone H1 to core histones to compare the total levels of H1 in different samples. To check these results with those of their gene expression, I used RT-qPCR and measured the transcript levels of different histone H1 subtypes: H1.0, H1.2 and H1.4. To analyze the morphological differences between the WT and KO ReN cells and the differential intranuclear localization of MeCP2 and histone H1, I used immunofluorescence.

The relationship between MeCP2 and histone H1 is important in a neuronal context as both proteins are highly abundant. The studies carried out so far on this topic have correlated the different quantity of H1 with the presence of MeCP2, the patterns of binding for the two proteins and their genomic binding locations. However, there have not been any studies on the question of whether MeCP2 has any bearing on the expression of different histone H1 subtypes. Different cell types, tissues and their developmental stages have characteristic patterns of H1 subtype expression. In this regard, it is interesting to determine if MeCP2 has any bearing on this in neurons. H1 subtypes have different chromatin binding affinities and different known and yet-to-be-known functionalities. Any indication of MeCP2 affecting H1 subtype abundances would be remarkable because of their differential role in shaping chromatin conformation[69].

1.7 Research hypotheses/questions and objectives

The objective of this study is to characterize a ReNCell VM cell system to be used as a model in further chromatin studies, addressing the MeCP2 and histone H1 transitions during cortical neuronal development. Previous results have shown that the amount of MeCP2 increases during this process[34,70,71] while histone H1 decreases approximately by half[50]. Also, Adrian Bird's lab has shown that the loss of MeCP2 in a MeCP2-KO mouse model was associated with the

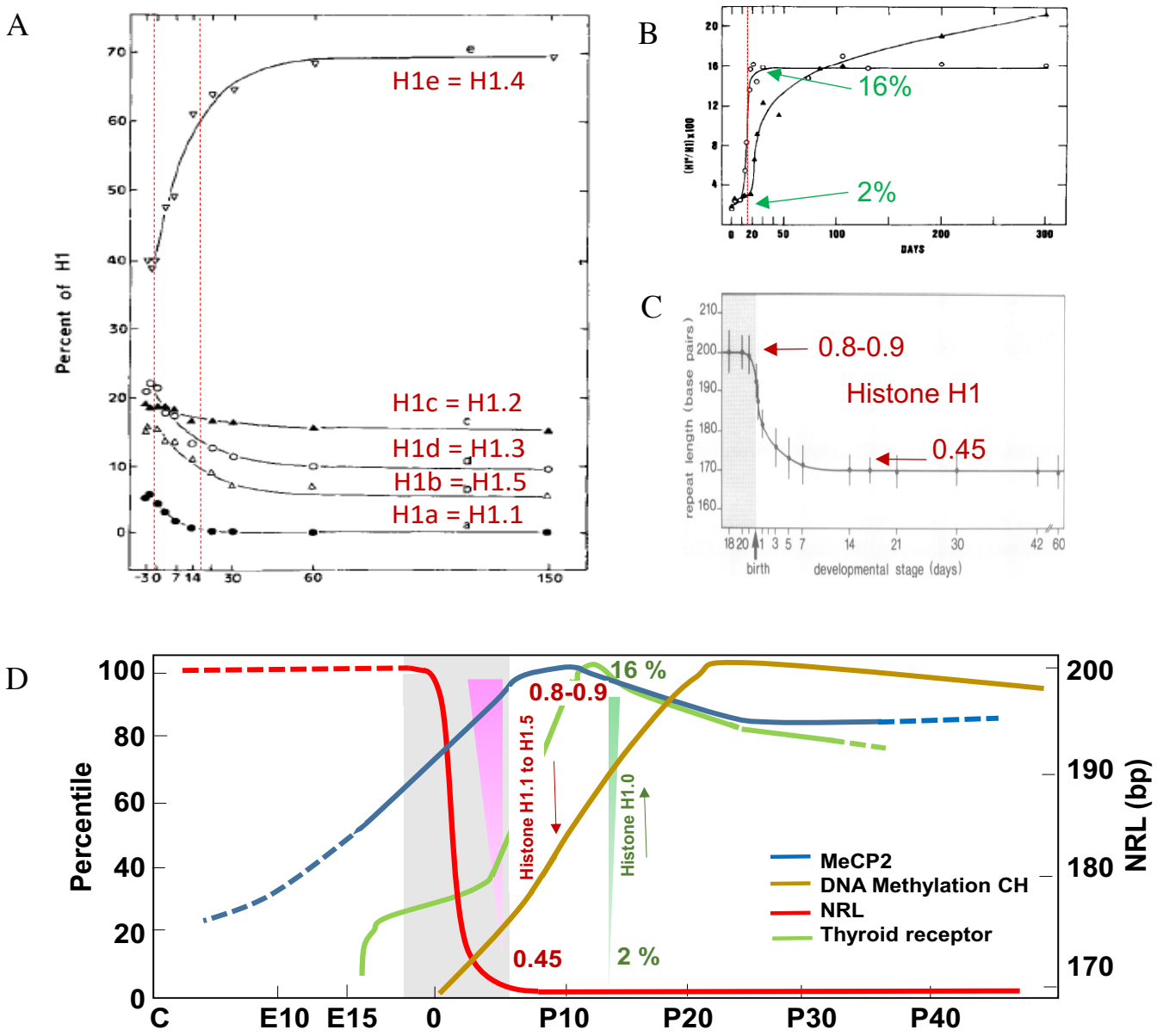

Figure 1. 6 Changes in chromosomal protein composition during murine brain and cortical neuron development. A) changes in histone H1.H1.5 subtypes during cortical neuron development in rats (from Fig.4 in Piña et al. (1987)[72]). **B)** Histone H1.0 change during rat cortical neuron development (Fig. 3 in Piña et al. (1984)[13]). **C)** The numbers in red indicate the decrease observed in histone H1 composition during the 200 bp to 160 bp NRL transition[49–51]. **D)** Figure summarizing the change in mouse MeCP2 during brain development[71,73] the postnatal DNA CH methylation in mice[52] and the changes in thyroid receptor in rat brain[74].

doubling of the neuronal histone H1 complement[53], suggesting that the increase of MeCP2 in WT is responsible for the decrease of histone H1.

Based on the evidence above, the hypothesis is put forward that *"in the course of development the levels of histone H1 in WT ReNCell will decrease compared to the MeCP2-KO ReNCell."*

Focusing on the different linker histone subtypes in the presence or absence of MeCP2 is highly relevant as no studies have been conducted to date in this regard. Because of MeCP2's involvement in chromatin rearrangement, it was also hypothesized that also *"the histone H1 subtype complement will change depending on its presence or absence."*

Chapter 2. Changes in chromosomal proteins during brain and neuronal cell development

2.1 Western blot analysis of mouse brain during development

To show that previous results regarding the expression trends of different chromosomal proteins during brain development can be replicated, the changes of histone H1.4 in mouse brains were analyzed. Our lab regularly uses CD1 (generic mouse strain) mouse tissues for western blots. Different ages were used to observe any changes along development: E14 (embryonic day 14), and several postnatal stages: P0 (day of birth), P4, P15 and P30. Along with mouse brains, P30 MeCP2-KO brains and their WT counterpart, and mouse livers as a non-neuronal tissue were included. Before looking at histone H1 subtypes, the changes in the level of MeCP2 were analyzed as our lab has previously extensively looked at this protein and observed a well-defined increase during development[13,35]. As the brain matures, there is an increase of MeCP2 with neuronal differentiation and subsequent maturation (Fig. 2. 1).

Next, the linker histone variation for two different subtypes, H1.0 and H1.4, were analyzed. Previous reports haven shown how neurons drop their level of histone H1 subtypes 1-5 during early differentiation[72] whereas they experience an increase in H1.0[13]. Histone H1.4 was chosen as a representative of subtypes H1.1 – H1.5 because it is the most abundant replication-dependent histone H1 subtype in neurons[72,75]. Hence, the expectation was to see an increase in H1.0 while H1.4 decreases. As previously shown, MeCP2, and H1.0 increased during brain maturation (Fig 2.1 and 2.2). There is no difference in the level of histone H1.0 between MeCP2-KO and WT brain. Although the brain has many other cell types besides neurons that do not experience an increase of MeCP2 or H1.0, whole brain extract still shows an increase for both proteins along development (Fig. 2. 1 and 2A); therefore, it was hypothesized that the H1.4

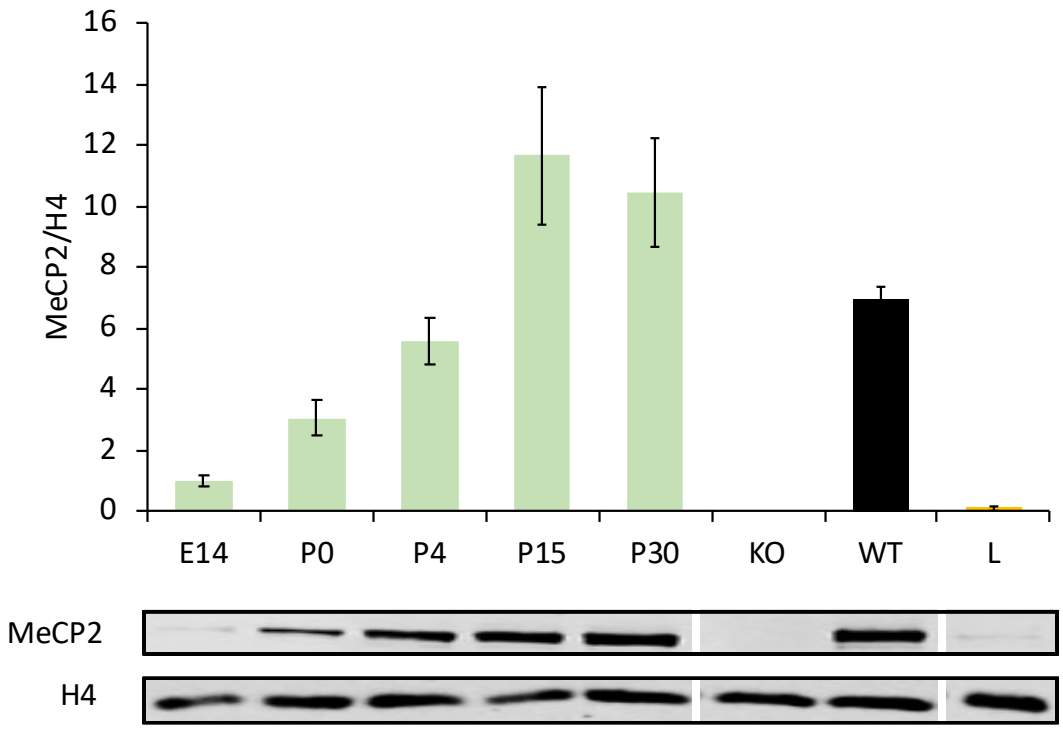

Figure 2. 1 MeCP2 increases during brain development. CD1 brains (E14 to P30, n=1), MeCP2-KO and colony control WT P30 brains (n=2) and P30 mouse liver (n=2). MeCP2 levels were normalized using histone H4. Graphs show averages of technical (for CD1 brains) and biological replicates ('KO' and 'WT' brain, and liver). Error bars represent standard error of the averages of the technical (for CD1 brains) biological replicates (for KO, WT and L). Representative westerns are shown below the graphs. The vertical white lines in the westerns separate different regions from the same western that were brought together to generate the final figure.

change observed in neurons would also be visible in the whole brain tissue. To this end, a western blot for H1.4 was carried out. However, changes with H1.4 along with age were not observed as would be expected from Figure 1. 6A. However, such an increase in H1.4 in this figure might be the result that at the time the data for Figure 1. 6A were generated[72], the global decrease in H1.1 – H1.5 shown in Figure 1. 6C had not been taken into consideration and hence the increase (if any) in H1.4 as shown in Figure 1. 6A might have been lower. Part of the inconsistency observed with H1.4 (Fig. 2. 2B) could also be attributed to the observed lower

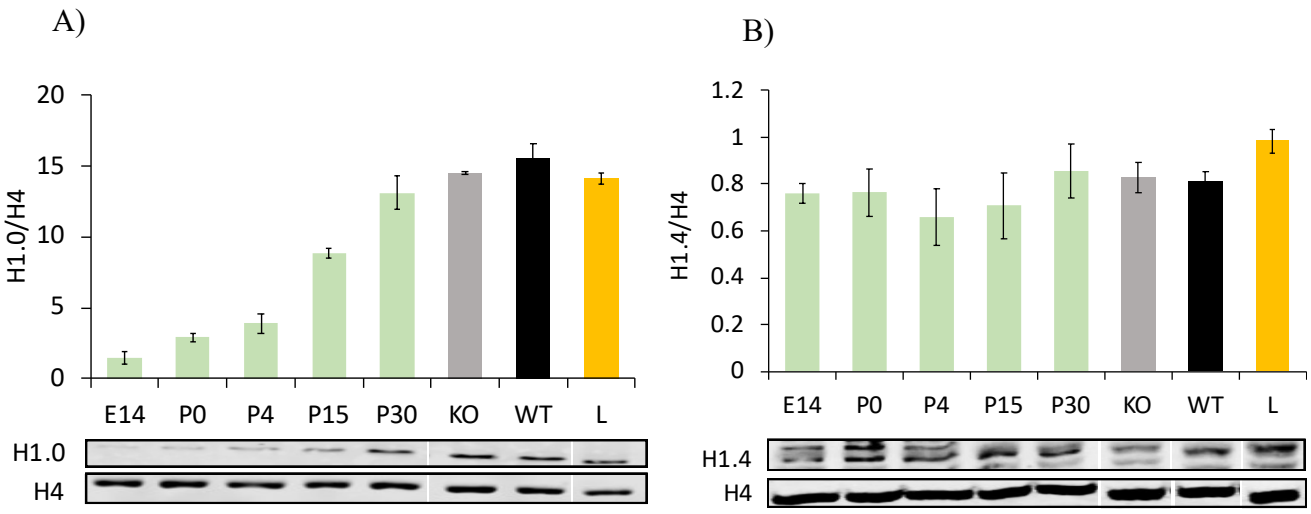

Figure 2. 2 Whole brain tissues show an increase of histone H1.0 during development but no change in the level of histone H1.4 Quantitative western blot of mouse CD1 brains (E14 to P40, mean +/- standard error of 3 independent experiments), MeCP2-KO and colony control WT brains (n=2) and P30 mouse liver (n=2) for **A)** H1.0 and **B)** H1.4. Histones H1.0 and H1.4 levels were normalized using histone H4. Graphs show averages of technical and where applicable, biological replicates. Error bars represent standard error of the averages of the biological replicates. Representative westerns are shown below the graphs. The vertical white lines in the westerns separate different regions from the same western that were brought together to generate the final figure.

quality of the H1.4 antibody for quantification purposes. Once the preliminary results were obtained using whole brain tissue, it was decided to use ReNCell which I expected would give us a clearer visualization of what happens with H1.4 in the presence and absence of MeCP2 and because of the availability of an MeCP2-KO for this cell line which could be extremely useful to test whether the presence of MeCP2 is responsible for the decrease observed in neurons

2.2 Characterization of WT and MeCP2-KO ReNCell during differentiation

2.2.1 Western blot analysis

The level of MeCP2 in WT ReNCell at multiple time points after differentiation was analyzed and an increase of MeCP2 was observed along the process until 8-12 DIV, at which point MeCP2 started to decrease (Fig. 2. 3A). Our collaborators in Spain obtained similar results (Fig. 2. 3C). When they compared the progenitor cells before induction of differentiation and 30 days post-differentiation, the level of MeCP2 exhibited a dramatic drop. For the scope of this project, however, the primary concern was the effect of MeCP2 on histone H1 subtype levels. Therefore, it was important to find a time point where the level of MeCP2 was high. When the results of Figure 2. 3A were compared to those of our collaborators', it was noticed that the point at which the level of MeCP2 is the highest occurs also at around 8 DIV. By comparing the results of the western blots with ReNCell WT at 0 DIV and 8 DIV, an increase in the level of MeCP2 of approximately 5 to 6-fold (Fig. 2. 3B) was observed. This increase is very similar to that described by Jung et al. (2003) using SHSY5Y, PC12 and NG 108-15 cell lines that can also be induced to differentiate *in vitro* into neuron-like postmitotic cells[70]. A preliminary study carried out at the time when ReNCell was first generated showed that while the ReNCell proteome changes from the proliferating stage to 4 DIV were vast, these changes became smaller from 4 DIV to 7 DIV[76]. Therefore, for all subsequent studies, it was decided to set 8 DIV as the end point of the differentiation studies.

Histone H1.0 is a differentiation specific marker particularly in cells undergoing terminal differentiation. Therefore, it was decided to check if ReNCell would show an increase of H1.0 as the cell progresses in differentiation. Though the western blots show that H1.0 is present in

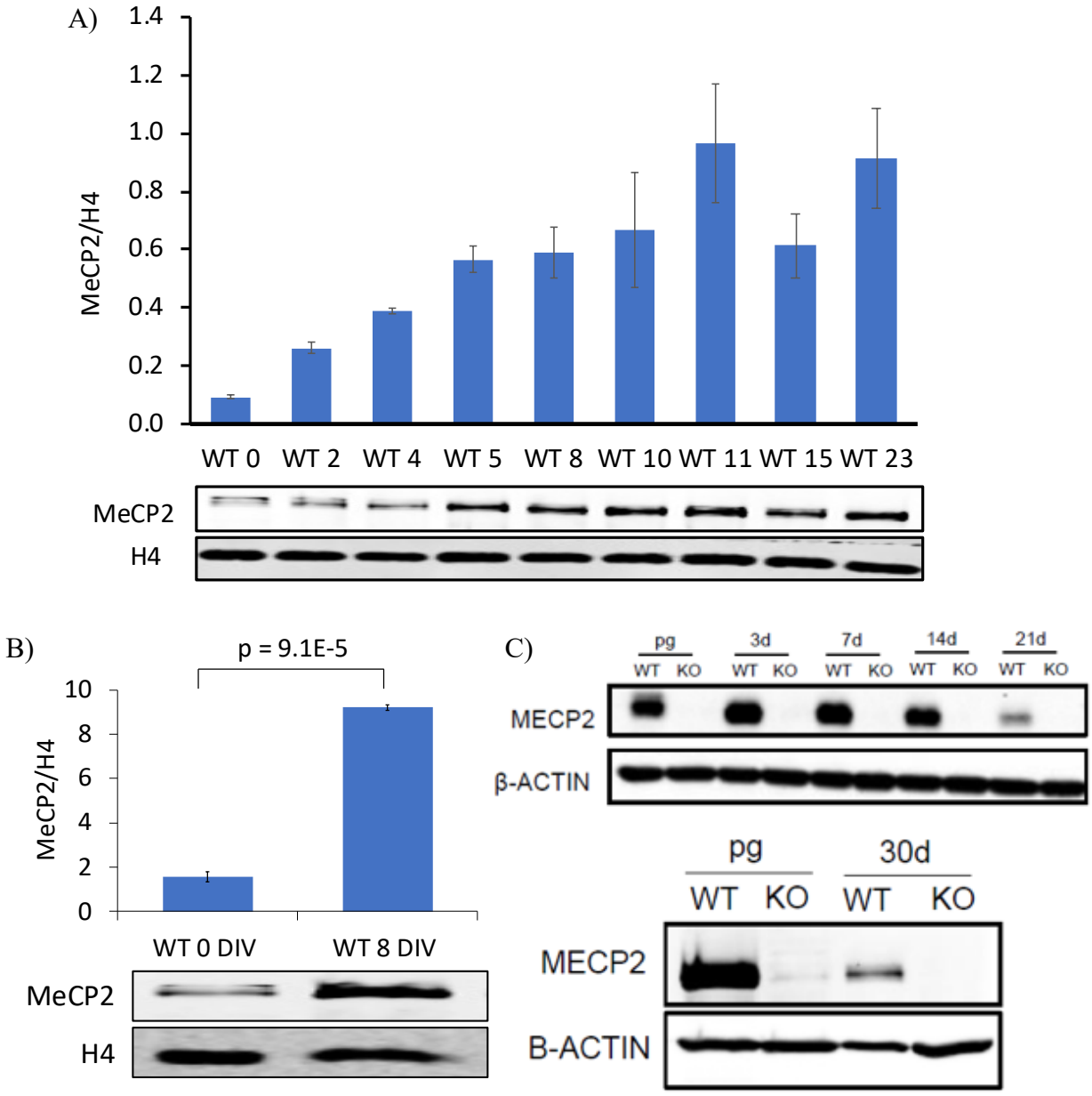

Figure 2. 3 MeCP2 increases after ReN cells are induced to differentiate. A) Quantitative western blot of ReNCell at different DIVs to assess MeCP2 levels. MeCP2 levels were normalized using histone H4 in both A and B. Graph shows mean +/- standard error of 3 independent experiments. Representative westerns shown below the graph. **B)** Comparative analysis of the difference in MeCP2 levels between WT 0 DIV and WT 8 DIV using data from quantitative western. Graph shows mean of 3 biological replicates and standard error. Two sample t-test assuming unequal variances. Representative westerns are shown below the graph. **C)** Data from our collaborators showing the decrease of MeCP2 along differentiation. MeCP2 levels were normalized using B-actin (data shown with permission). Pg: progenitor cells (0 DIV).

mouse brain and liver, neither the WT nor the KO ReN cells show detectable levels of H1.0 even at 24 DIV (Fig. 2. 4). Though this may have been due to the antibody being specific for the mouse isoform of H1.0 while ReNCell is a human sample, the Western images from HPLC results shown later clearly indicate that H1.0 antibody can detect human H1.0 in other human cell lines (Fig. 2. 8B). Hence, it seems that H1.0 is not detectable in the WT ReNCell and only trace amounts can be visualized in the MeCP2-KO cells (Fig. 2. 4). As ReNCell was derived from human embryonic fetal tissue, an increase in the level of H1.0 had initially been predicted to occur along differentiation. Therefore, its absence in all of the ReNCell types was surprising.

An early concern when considering the use of WT and MeCP2 deficient ReNCell was that the absence of MeCP2 in the latter could affect the neural differentiation of these cells. MeCP2 is a protein involved in maintaining the differentiated state of neurons[38]. A previous report shows that neural cells without MeCP2 are underdeveloped with less complex arborization[38]. Another report indicates that the absence of MeCP2 encouraged the neural progenitor cells to differentiate into non-neuronal cells[77]. However, neurons differentiate to a certain extent in a MeCP2-KO mouse[38]. Yet, the absence of MeCP2 affecting the cell fate of MeCP2-KO ReNCell compared to the WT counterpart could be concerning if all what being compared were simply two different cell types as opposed to two cell lines merely differing in the presence of MeCP2. As the focus of this project is on neurons and the previous reports on MeCP2 and histone H1.4 used as a reference (Fig. 1. 6) are also pertinent to neurons, it was imperative to check the two cell types for their ability to undergo proper neuronal differentiation. To confirm this, a western analysis was performed using NeuN, a marker found in neuronal nuclei that is often used for this purpose. The NeuN western results showed that KO cells

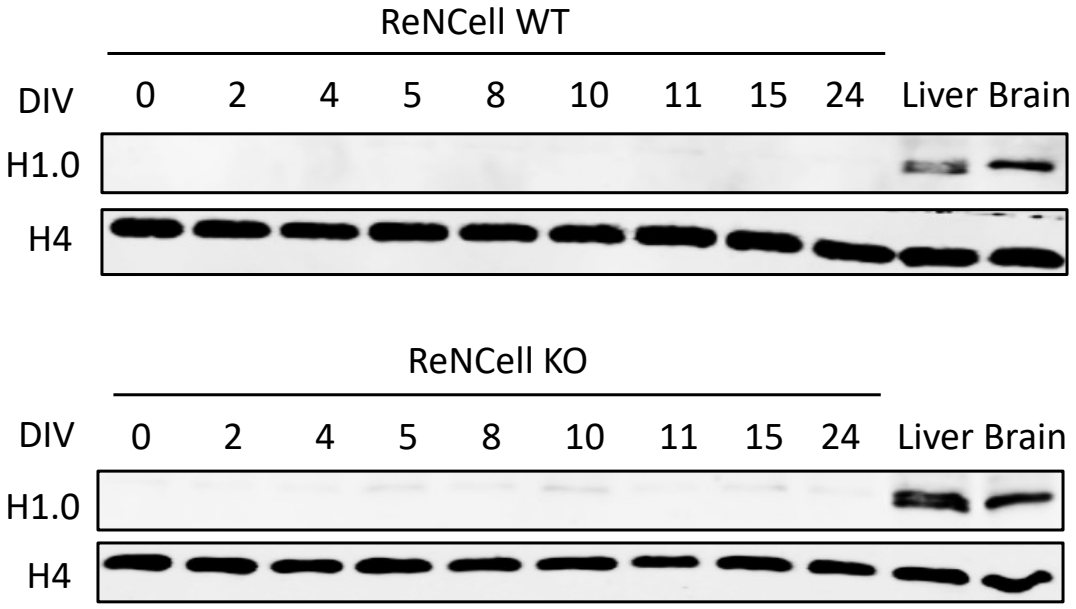

Figure 2. 4 Histone H1.0 is undetectable in both ReNCell WT and KO. Histone H1.0 levels were normalized using histone H4. Mouse liver and brain samples were used as positive controls.

had more NeuN than the WT (Fig. 2. 5) which is interesting in light of previous studies mentioned earlier regarding MeCP2's involvement in neuronal differentiation. However, it was decided not to pursue this any further as the NeuN westerns were simply used to confirm that ReNCell KO is differentiating into neurons.

Next, an attempt was made to compare H1.4 levels between WT and MeCP2-KO via quantitative western blots. It is difficult to find specific H1 subtype antibodies as replication-dependent histone H1 subtypes are very similar in sequence (Fig. 1. 2). As suspected, quantitative westerns for histone H1.4 were difficult because the results obtained varied with the different H1.4 antibodies and within technical replicates. Therefore, only inconclusive western results could be gathered.

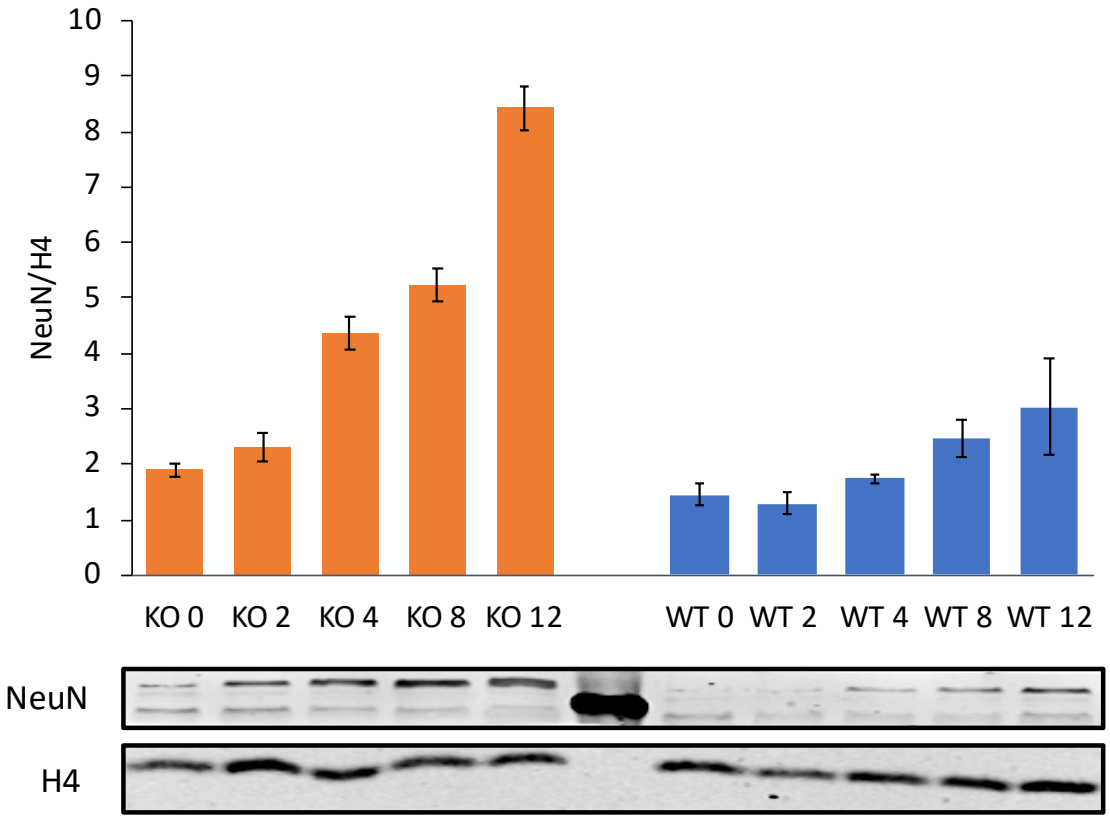

Figure 2. 5 Both WT and KO ReNCells express NeuN. NeuN levels were normalized using histone H4. Graphs show averages of three technical replicates. Error bars represent standard error of the averages of three western technical replicates. Representative westerns are shown below the graphs.

2.2.2 HPLC characterization of linker histones in WT and MeCP2-KO ReNCell

Because I was interested in studying the potential relation between histone H1 and MeCP2 and because of the negative results with histone H1.4 obtained in the previous section, it was decided to change the strategy and to use an HPLC approach rather than western quantification in order to compare the overall histone H1 levels between WT and MeCP2-KO ReNCell. To this end, I decided first to use HPLC which allows for the separation of linker histones from core histones in a way that allows for the quantification of the total level of histone H1 and relate it to the total amount of core histones. It was also decided to look at the transcript

levels of histone H1 subtypes in the two cell types. Using subtype-specific primers, it was possible to quantify and compare the transcripts of different H1 subtypes in WT and MeCP2-KO ReN cells.

In order to have fractions of increased purity for HPLC analyses, nuclei were first purified and the histones were further extracted using hydrochloric acid. Figure 2. 6 shows a comparison between the total chromosomal proteins in the nuclear extracts before and after HCl extraction and Figure 2. 7 shows the HCl extracts of all the samples used in HPLC. Because histones are positively charged proteins, they are easily extracted with acids, and this provides an enhanced purity of these proteins as it is clearly shown in Figure 2. 6. As it can be seen in this figure, many proteins in the non-histone regions of the gel are removed. This figure also shows that the histone H1 subtype composition seems to differ between mouse tissues (brain and liver) and human immortalized cell lines (HEK and HeLa). In the linker histone regions of the gel in mouse brain and liver, there is one prevalent lower mobility band while in HEK and HeLa, there are two major bands shown in the same region. This different composition in linker histones may be attributed to the species differences or to the fact that HEK and HeLa are immortalized cell types that are continuously dividing.

With the proper optimization of the eluting solvent phase and columns, RP-HPLC can be used to separate linker histones from core histones[78]. Further optimization of the procedure was required to standardize the amount of sample loaded onto the column that was required to obtain an optimal separation of the proteins. Even though large amounts of sample could be useful in providing more protein in the fractions,

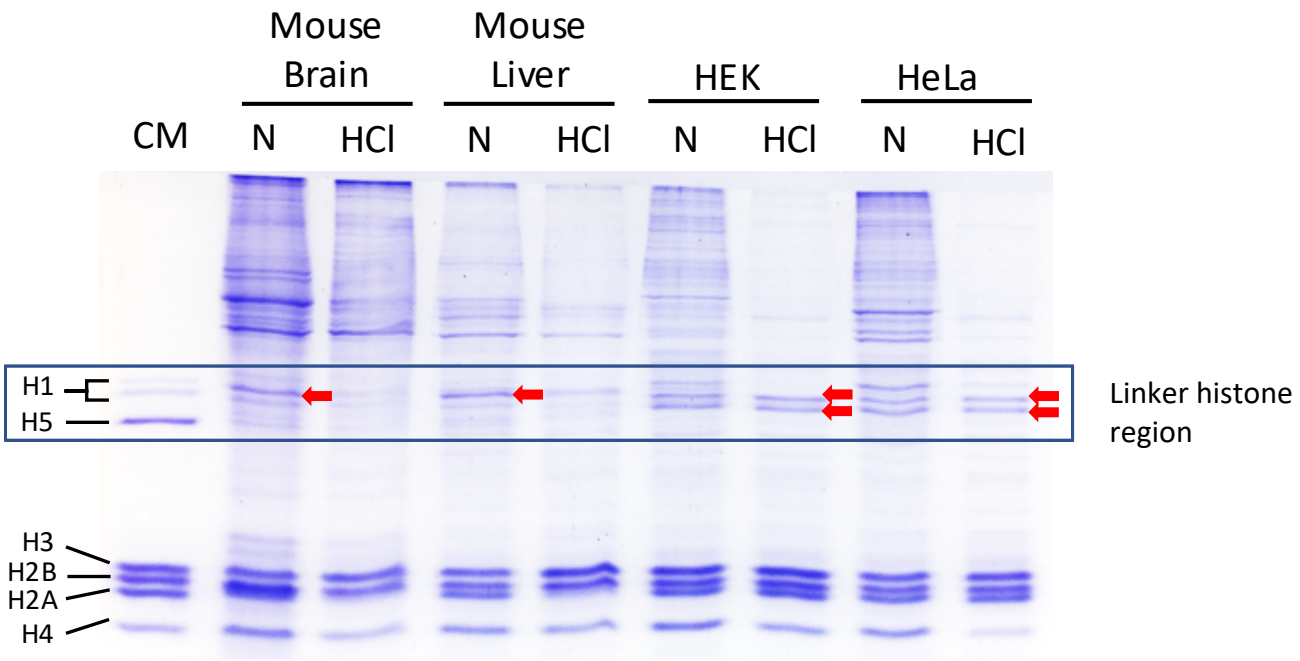

Figure 2. 6 HCl extraction after nuclear extraction yields a more pure sample of histones. Mouse brain and liver as well as HeLa cells were used as a comparison. The arrows point to the most prevalent band(s) observed in the linker histone region of the gel.

analysis while producing good resolution of peaks in the chromatogram. For this optimization, HCl-extracted histones from chicken erythrocytes, mouse liver and HeLa cells (Fig. 2. 8) were used. Although mammalian erythrocytes lose their nuclei at the late stages of differentiation, the birds' erythrocytes retain their nucleus and thus it is possible and easy to obtain HCl-extracted histones from chicken erythrocytes and they are regularly used in our lab as histone markers. Other samples also used to compare with the ReNCell samples included mouse that can compromise the separation resulting in the merging of the peaks visualized in the chromatogram. Therefore, it was imperative to determine the optimal range of protein to be loaded that is large enough to produce fractions amenable for both western blot and SDS-PAGE liver HCl extract

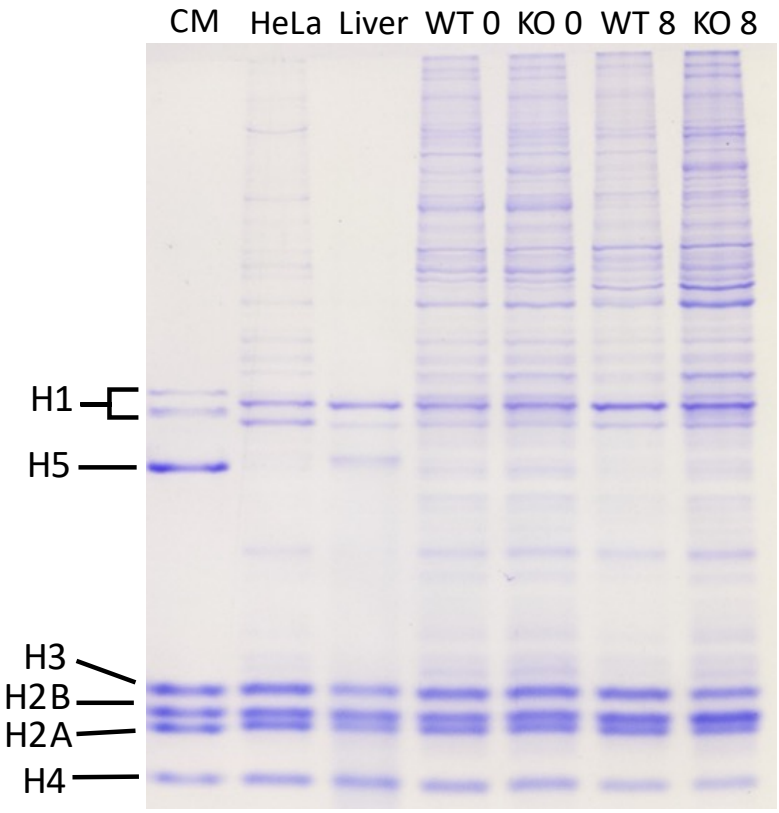

Figure 2. 7 Coomassie-stained SDS-PAGE of the HCl-extracted histones from the samples to be injected into HPLC. CM = chicken histone marker as in Figure 2. 6.

as a tissue control and HeLa HCl extract as a human cell control which as with ReNCell, is also an immortalized cell line. All the control samples were processed in two steps as described earlier: nuclear extraction and then HCl extraction. However, for ReNCell samples, due to the limited amounts of cells available, the HCl extraction was carried out using a slightly simplified version of the nuclei preparation (see Materials and Methods).

The HPLC chromatograms of all the different cell extracts used (Fig. 2. 8) show that linker histones are eluted at fractions 40-45 and then the core histones are eluted thereafter. The linker histones generally elute in two major peaks whereas core histones are present in six peaks, where the last two correspond to the H3 dimers which dimerize through disulfide bonds due to

the unique presence of cysteine in this histone. The different HPLC fractions were collected and loaded onto SDS-PAGE for Coomassie staining and for western blots using H1.0, H1.2 and H1.4 antibodies (Fig. 2. 8B). For the H1.4 western blots with HPLC fractions, a more specific antibody, different from the one used previously in my early westerns with total cell extracts, was used.

Similar to the results obtained from Figure 2. 4, the western blots of the HPLC fractions of ReNCell did not show any detectable levels of histone H1.0. Histone H1.0 is also a conserved subtype and because the H1.0 antibody was able to blot the H1.0 found in HeLa (Fig. 2. 9B, "HL"), which is another human cell line, I was able to confirm that this was not an antibody problem. Even though H1.0 is well-known for its abundant presence in terminally differentiated cell types, H1.0 has also been shown to be present in embryonic mouse tissues albeit at lower amounts[75]. Therefore, it is surprising that ReNCell does not contain H1.0 and if it does, this is at extremely low levels.

In all the ReNCell samples, two major H1-containing peaks can be observed in the linker histone region (Fig. 2. 8). H1.2 was systematically eluting in fewer fractions than H1.4 (Fig. 2. 8B). The elution patterns of H1.2 and H1.4 differ between WT and KO. In the WT, H1.2 elutes in one fraction and is seen as two bands at 0 DIV and 8 DIV. However, in KO, H1.2 elutes in two separate fractions, mainly as a single band (the lower one). By contrast, H1.4 was eluted in two fractions in WT ReNCell whereas it was eluted over several fractions in MeCP2-KO ReNCell. The different elution of H1.4 could be an indicator of different PTMs associated with histone H1.4 which would be dependent on the presence of MeCP2. These subtype-specific westerns cannot be used for quantification of each subtype as there is no way of normalizing

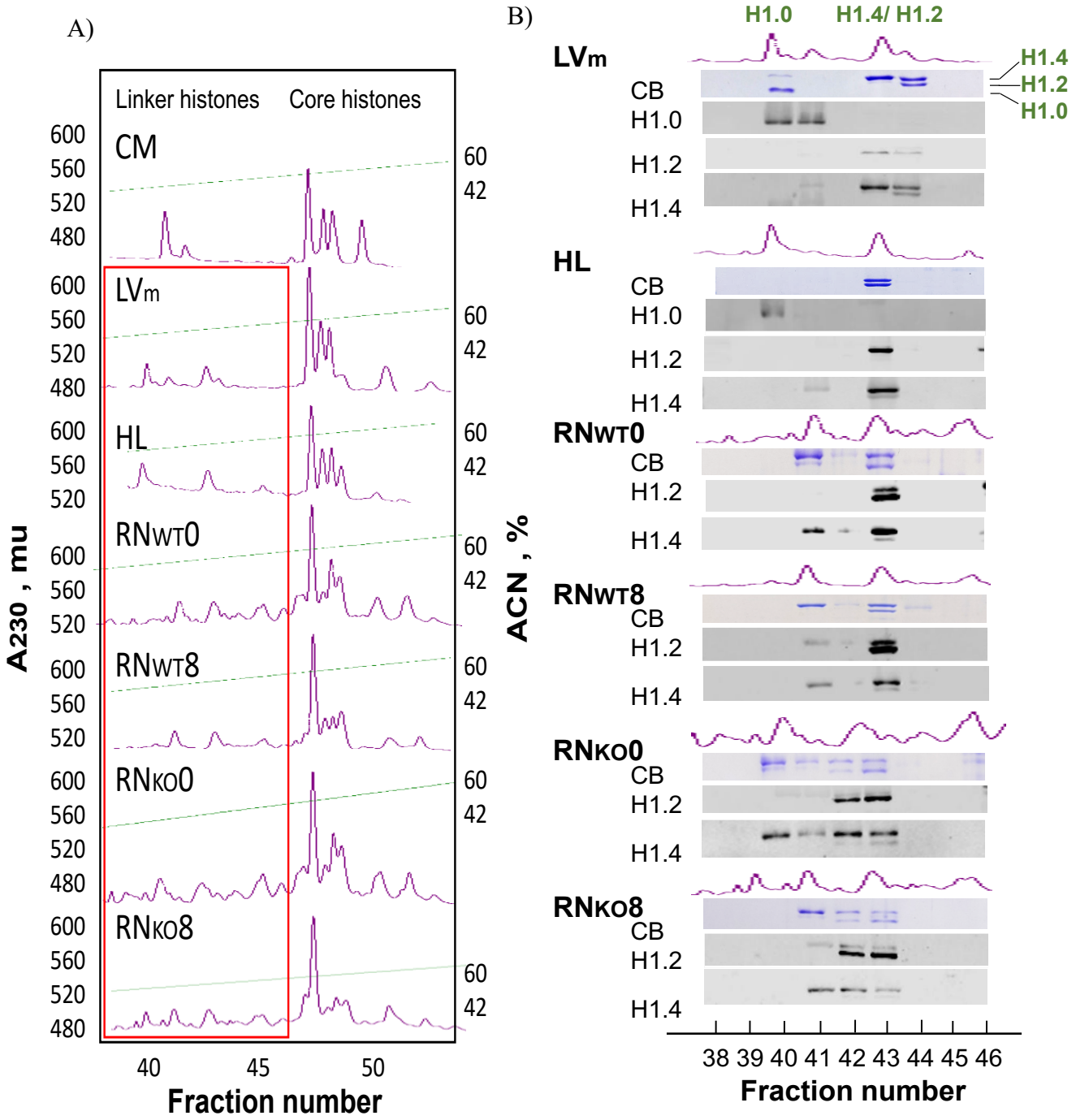

Figure 2. 8 The biochemical profiles of linker histones differ depending on the presence or absence of MeCP2 in ReNCell. A) HPLC chromatograms of ReNCell and other samples used for comparison. Early fractions (#40-45) show the linker histone peaks and later fractions (#45-50) correspond to the core histone peaks. **B)** The fractions collected from RP-HPLC were run on SDS-PAGE for Coomassie staining (shown in blue) and western blotting for histone H1 subtype (shown in black and white). Corresponding fractions are shown as chromatogram above. A_{230} = absorbance at 230 nm, mAU = milli absorbance units, ACN = acetonitrile, LVm = mouse liver, HL = HeLa, RN = ReNCell, CM = chicken erythrocyte histones.

the intensities of the bands. Nevertheless, in the chromatograms (Fig 2. 8A), it is possible to add all the areas of the peaks in the linker region by using the integration software of the HPLC program and normalize them with respect to the area of the peaks corresponding to the core histone region in order to determine the relative total linker/core histone level (Appendix A). When the ratios of total H1 to total core histones of all the samples used in HPLC were calculated, the chicken erythrocytes had the highest value, as expected from Table 1. 1 (Fig. 2. 9A). Of the many tissues and cell types compared in the past for their linker to core histone ratios, chicken erythrocytes are reported to have the highest because of their histone H5 content. Histone H5 is a homologous subtype of the mammalian H1.0[79] and mature chicken erythrocytes, like those of the nucleated erythrocytes from fish, amphibians, and reptiles[80], contain high levels of histone H5. The next highest linker-to-core histone containing sample was MeCP2 deficient ReNCell differentiated for 8 days (Fig. 2. 9). However, the difference between WT and MeCP2-KO ReNCells at 8 DIV is not statistically significant and neither is the difference at 0 DIV.

Similar analysis of the linker histone/core histone ratio was performed using the densitometrically scanned images of the SDS-PAGE shown in Figure 2. 8. The results thus obtained (Fig. 2. 9B) show similar results as those from HPLC (Fig. 2. 9A). The linker histone/core histone ratios obtained from the two methods (Fig. 2. 9) were averaged and converted onto estimated molar ratios using CM as a reference (Table 2. 1). These data clearly indicate that in ReNCell, the levels of histone H1 remain similar although a non-statistically significant trend to increase appear to be present in KO cells at 8 DIV.

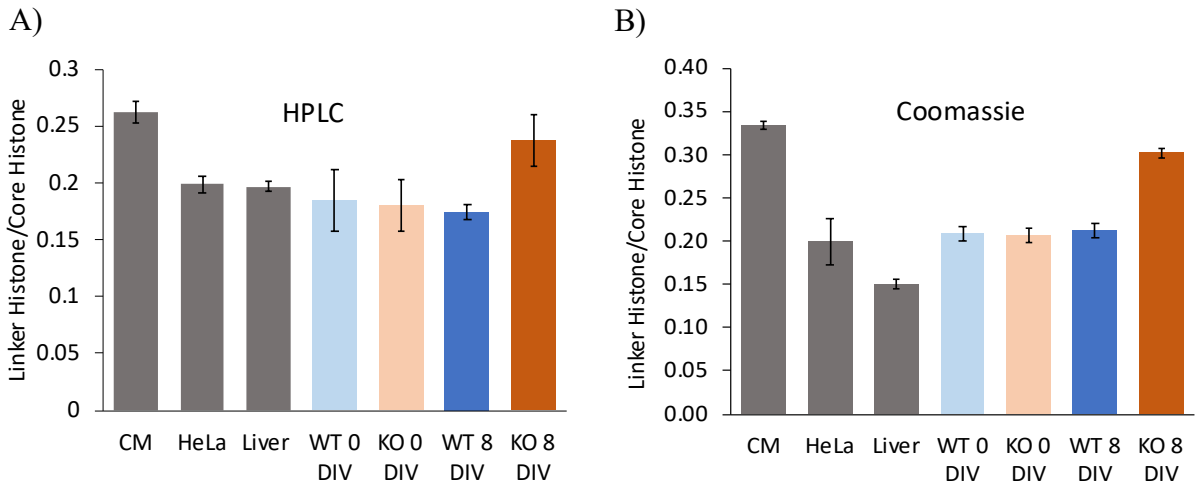

Figure 2. 9 There is a trend of a higher level of linker histones in MeCP2-deficient ReNCell at 8 DIV. A) The ratio of linker histones to core histones calculated by quantifying signals from HPLC chromatograms. **B)** the ratio of linker histones to core histones calculated by quantifying the Coomassie-stained bands in Figure 2. 7. Data represent mean of 3-5 independent experiments ± standard error. Two sample t-test assuming unequal variances between WT and KO show that the difference at each time point is insignificant.

Table 2. 1 Histone H1/core histone ratios of various samples as shown in Figure 2. 9. The averages of Coomassie and HPLC values were converted into molar ratios using a value of 1.3 mol linker histone/mol histone octamer (Table 1. 1) for chicken erythrocyte.

Sample	Histone H1/ core histone (Average of Coomassie and HPLC)	Estimated mol histone H1/ mol octamer
CM	0.298	1.3
HeLa	0.199	0.87
Mouse liver	0.174	0.76
WT 0 DIV	0.197	0.86
KO 0 DIV	0.194	0.84
WT 8 DIV	0.193	0.84
KO 8 DIV	0.27	1.18

2.3 Determination of the different levels of histone H1 subtype gene expression

While HPLC allowed the observation of linker and core histones' relative composition in different tissue and cell-type samples, RT-qPCR was used to quantify the transcript levels of the H1 subtypes. For RT-qPCR, I decided to focus on H1.0, H1.2 and H1.4. It was of interest to see what would be the H1.0 transcript level in ReN cells even though histone H1.0 was undetectable at the protein level. It was also of interest to check whether the H1.2 and/or H1.4 transcript levels would be different in the absence of MeCP2. Although the HPLC results (Fig. 2. 9) showed that the total histone H1 levels were not significantly affected by the presence of MeCP2, the transcript levels of each histone H1 subtype could be different and if so, would suggest a control mechanism at the level of translation. The levels of the three chosen histone H1 subtype transcripts were normalized using GAPDH and RPLP0. As in the HPLC analysis, ReNCell WT and KO at the same two time points, 0 DIV and 8 DIV, were compared. Despite the lack of statistical significance, all three transcripts at 0 DIV were more abundant in WT ReN cells (Fig. 2. 10). This is unlikely to be due to chance.

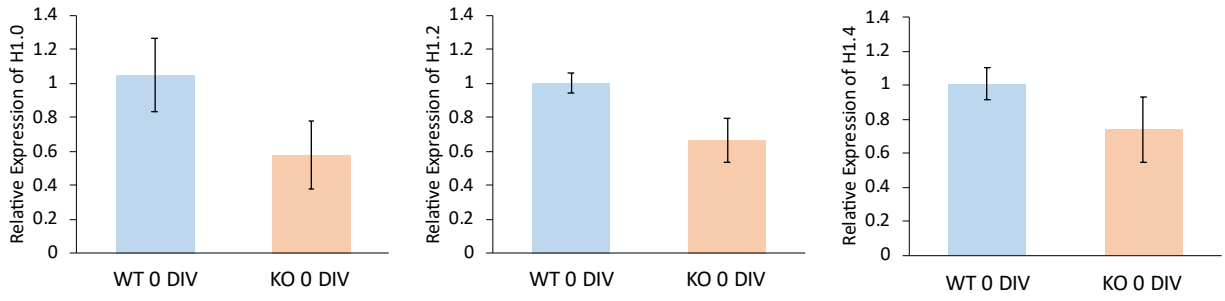

Figure 2. 10 All three histone H1 subtypes (H1.0, H1.2, H1.4) show a higher level of transcripts at 0 DIV in WT ReNCell compared to MeCP2-KO cells. Histone subtype (H1.0, H1.2, H1.4) transcripts were quantified via RT-qPCR. RT-qPCR data were analyzed using the geomean of the Geomean Pfaffl method (n=3). Data represent mean of three biological replicates ± standard error. Two sample t-test assuming unequal variances for each graph showed no significant differences between WT 8 DIV and KO 8 DIV.

Even though previous studies show that histone H1 increases in developed cortical neurons of MeCP2-KO mice, there have been no previous studies carried out on histone H1 transcripts of proliferating neural progenitor cells comparing to their MeCP2-KO counterpart. Therefore, the results in WT and MeCP2 deficient ReNCells at 0 DIV is a novel and notable observation. At 8 DIV, H1.0 and H1.2 transcript levels do not seem to have any changes in the absence of MeCP2 (Fig. 2. 11) and it is the H1.4 level at 8 DIV which shows the most difference. However, none of these differences are statistically significant.

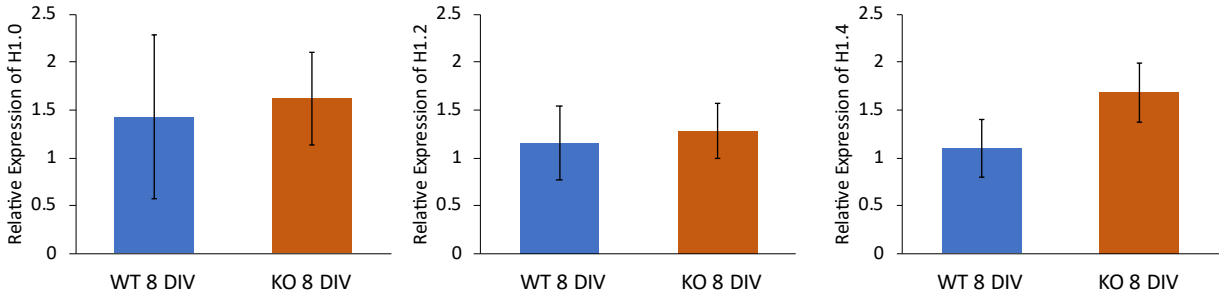

Figure 2. 11 There is no difference in the levels of histone H1.0, H1.2 or H1.4 transcrips between WT and MeCP2-KO ReNCell at 8 DIV. RT-qPCR data were analyzed using the geomean of the Geomean Pfaffl method (n=3). Data represent mean of three biological replicates ± standard error. Two sample t-test assuming unequal variances for each graph showed no significant differences between WT 8 DIV and KO 8 DIV.

Similar to what was observed for the H1.0 protein levels in ReNCell, histone H1.0 transcripts were also expressed at lower levels than H1.2 and H1.4. In fact, H1.2 was expressed at 85-fold higher levels and H1.4, 443-fold higher level compared to H1.0 (Fig. 2. 12). These fold expressions of H1.2 and H1.4 subtypes compared to H1.0 were similar in all ReNCell samples used in the RT-qPCR analysis (Appendix E).

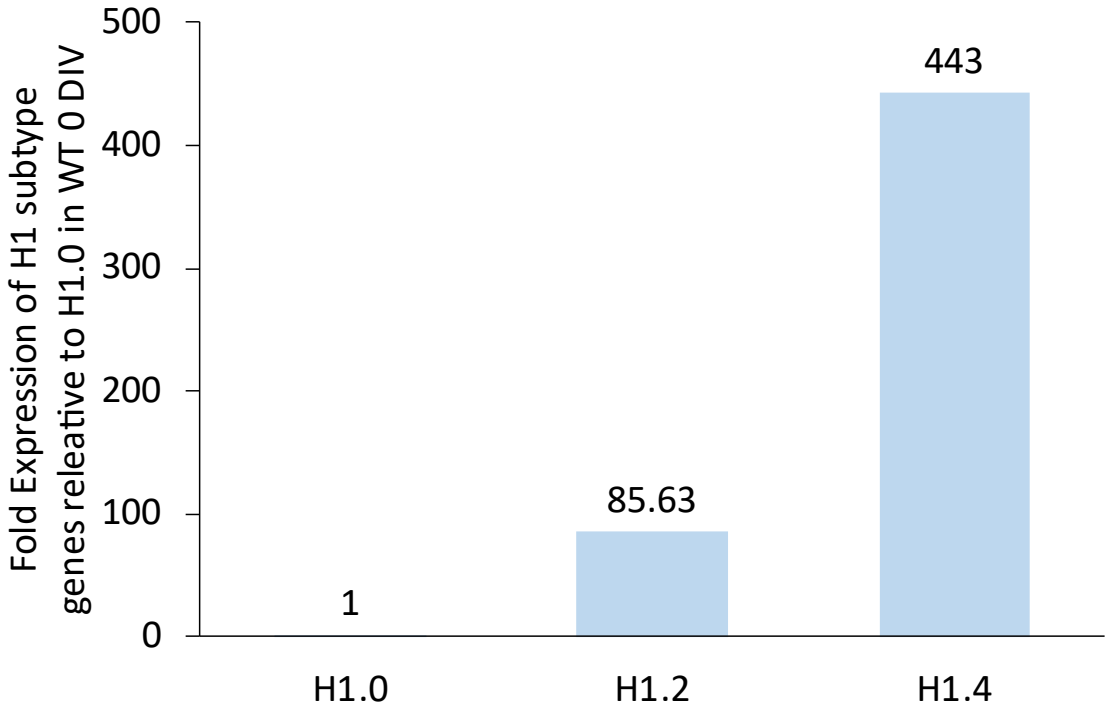

Figure 2. 12 Histone H1.4 is the highest-expressed linker histone subtype. For similar comparisons in other ReNCell samples, see Appendix E.

Chapter 3. Cytological characterization of WT and MeCP2-KO ReNCells

3.1 Immunofluorescence analysis of cell morphology

In the process of culturing ReNCell, some morphological differences between the WT and MeCP2-KO cells were noticed. Therefore, a plasma membrane dye SGC5 in combination with a DNA-binding dye (DAPI) for the nucleus was used to observe the cell morphology using fluorescence microscopy. At 0 DIV, compared to WT ReNCell which seems to have a fibroblast-like morphology (Fig. 3. 1A), KO ReNCell's cell membrane does not extend from the nucleus (Fig. 3. 1B).

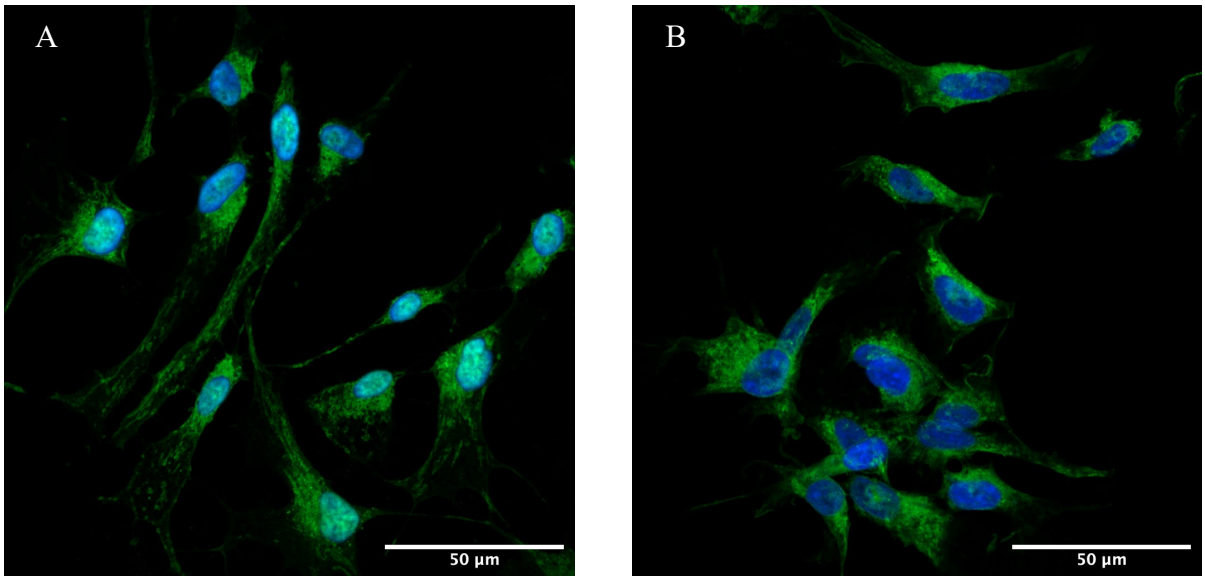

Figure 3. 1 WT ReNCell has a more elongated cell membrane and is less aggregated compared to MeCP2-KO cells at 0 DIV. Green = membrane dye. Blue = DAPI. **A)** ReNCell WT at 0 DIV. **B)** ReNCell MeCP2-KO at 0 DIV. Scale bars represent 50 μm.

Striking differences were observed between WT and MeCP2-KO cells when they were differentiated for 8 days (Fig. 3. 2). For ReNCell WT cells, SGC5 staining shows the elongated projections from the cell body corresponding to the dendrites and axons. These projections are thin and elongated in WT cells which is expected of properly differentiating neurons. The projections are also webbed, and this shows that the cells are in the process of establishing communication networks as it is observed in *in vivo* neuronal networks. Of note, the cell bodies of WT cells are smaller than those of KO cells. For MeCP2-KO cells, there is almost no elongation of the membrane. In fact, the membrane shows characteristics of preliminary differentiation as indicated by the stretching of the membrane in lamellipodia-like structures. The KO cells also seem to start initiating or establishing some connections amongst themselves.

Another big difference between WT and MeCP2-KO ReNCells other than the difference in cell morphology is in the separation of the cells (Fig. 3. 1 and 2). In culture, cells were

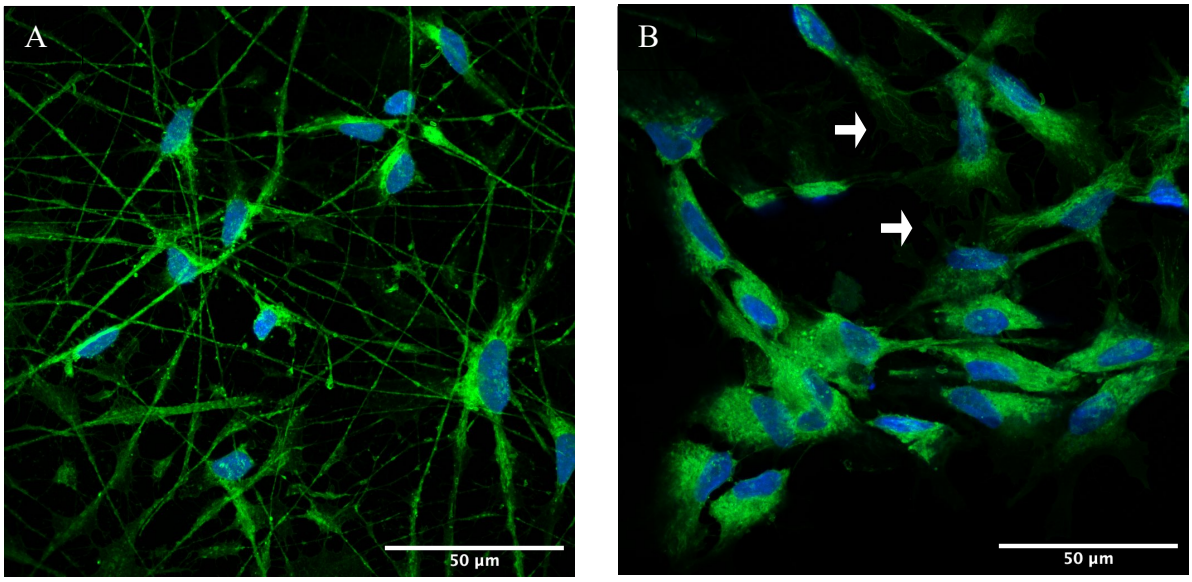

Figure 3. 2 WT and MeCP2-KO ReNCells have different morphology at 8 DIV with regards to membrane projections and cell spacing. Green = membrane dye. Blue = DAPI. **A)** ReNCell WT at 8 DIV. **B)** ReNCell MeCP2-KO at 8 DIV. White arrows point to lamellipodia.

seeded in a way that would keep them separated from each other. However, once the cells attached to the plates at 0 DIV and were differentiated to 8 DIV, KO cells tended to aggregate with each other. By contrast, WT cells grew spaced out from each other. This was noticed during the routine checks of the cells carried out with the light microscope and was also confirmed by subsequent IF images (Fig. 3. 1 and 2).

3.2 Visualization of MeCP2 in ReNCell

For the visualization of MeCP2 and histone H1.4, a rabbit H1.4 antibody, several MeCP2 antibodies and DAPI were used. The initial IF trial results with antibodies showed that though histone H1.4 showed nuclear localization, MeCP2 unexpectedly showed cytoplasmic localization (Fig. 3. 3). This was very surprising as MeCP2 should predominantly be present in the nucleus.

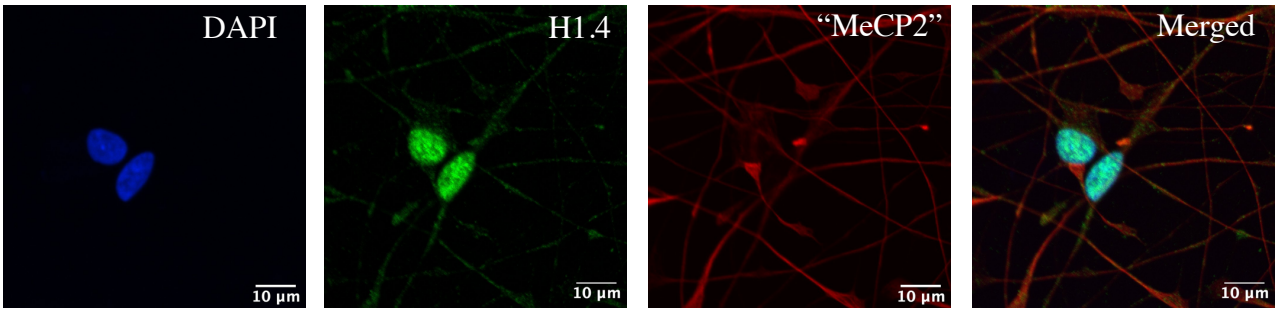

Figure 3. 3 WT ReNCell shows nuclear localization of histone H1.4 and extranuclear localization of MeCP2. The MeCP2 antibody used in this figure is a mouse antibody (M6818, Sigma-Aldrich) and the H1.4 antibody is a rabbit antibody (41328S, CST). Scale bars represent 10 μm.

Because of this, two other MeCP2 antibodies were tried, one of which was produced in mouse and the other in chicken. In a similarly unexpected way, these two antibodies also showed

a preferential cytoplasmic localization (Fig. 3. 4). The binding of these antibodies resembled that to be observed with cytoskeletal element antibodies because of their fibrous binding pattern.

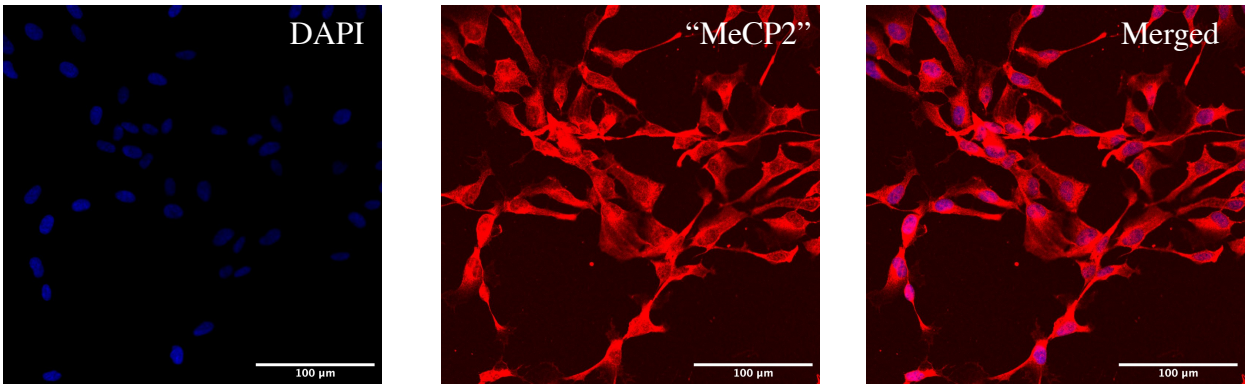

Figure 3. 4 MeCP2 staining using different antibodies fails to localize MeCP2 to the nucleus. ReNCell WT 0 DIV cells fixed and stained with DAPI and a mouse MeCP2 antibody (4B6, WH0004204M1). MeCP2 antibody displays a fibrous binding pattern (similar results were shown with the chicken MeCP2 antibody – results not shown). Scale bars represent 100 μm.

While the possibility exists that the secondary antibody could be causing off-target binding, this was unlikely to be the case given that the secondary antibody control showed no unspecific binding. Several considerations were made to fix this issue. In the past, our lab ran into similar problems with immunohistochemistry (with fixed mouse brain sections) where nuclear MeCP2 could not be properly visualized. Such problem was fixed at that time by modifying the fixation conditions[56]. Although the usual fixation conditions for immunocyto/histochemistry usually involve 4% PFA at pH 7.4, those conditions had to be modified to a fixation with PFA pH 6.5 for one hour followed by a post-fixation with PFA at pH 11[56]. Because this fixation condition had been optimized for tissue sections which have significantly larger permeability issues, I decided to shorten the fixation time for the cells on coverslips but use the same pH conditions. Another consideration for optimization was the

antibody titration. The starting antibody dilution was 1:500 and there was a possibility that this could be too high of an antibody concentration which could potentially result in non-specific staining. Because the immunofluorescence protocol often calls for a blocking step using serum, blocking was performed during the initial immunofluorescence trials; these initial results showed that there was no difference whether the coverslips were blocked or not, and hence blocking was not initially performed. Yet, in a further optimization attempt to solve the MeCP2 issue, blocking was checked once more. One explanation for this problem was that there was insufficient permeabilization and that antibodies were unable to cross the plasma and/or the nuclear membrane; however, this was unlikely given this problem was not observed with histone H1.4 that was localized specifically to the nucleus.

In the optimization experiment performed with HEK cells, the first MeCP2 antibody dilution I tried with these cells was 1:5,000. While some non-nuclear staining was still observed, the nuclear localization increased (data not shown). Because of this promising observation, a 1:10,000 dilution was tried next in combination with a different fixation and blocking condition. This was tried in combination with two different antibodies: one MeCP2 antibody produced in chicken (Fig. 3. 5) and another antibody produced in mouse (M6818, Sigma-Aldrich) (Fig. 3. 6).

Blocking did not cause much change although there seemed to be some improvements for the chicken antibody which targets the C-terminus of MeCP2. Nevertheless, there was more localization to the nucleus with the 1:10,000 dilution for both antibodies. This allowed us to confirm that the antibody dilution has a bearing on proper antibody localization and gave us the confidence that this dilution of the MeCP2 antibody would allow to properly visualize the protein at its nuclear location in ReNCell.

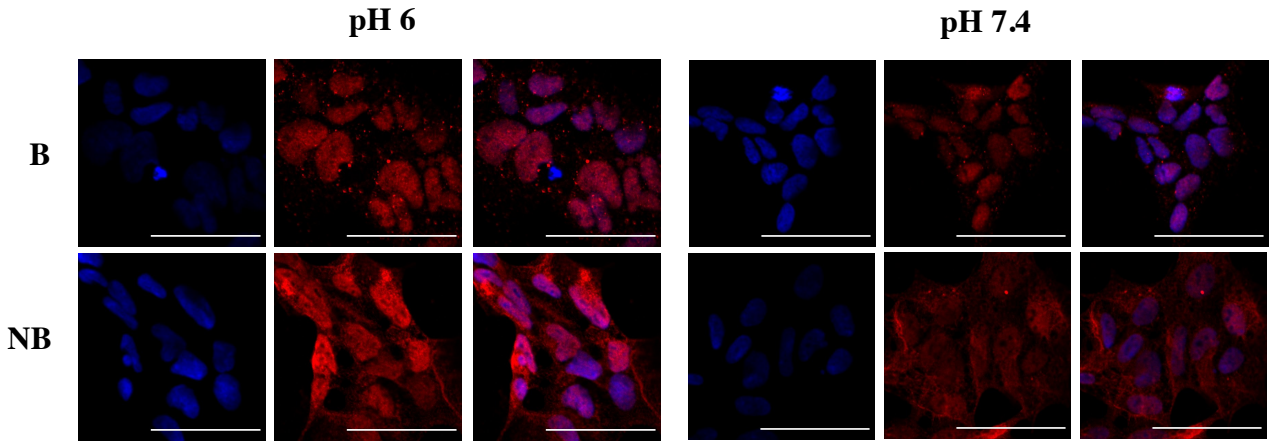

Figure 3. 5 Imaging of HEK cells processed under different conditions using a chicken MeCP2 antibody show an enhanced localization of MeCP2 to the nucleus. HEK cells were fixed with either pH 6.5 (left three columns) or pH 7.4 PFA (right three columns) and blocked (B) or not blocked (NB). After fixation and blocking (where applicable), HEK cells were stained with 1:10,000 anti-MeCP2 antibody produced in chicken. Blue = DAPI, Red = MeCP2. Scale bars represent 50 µm.

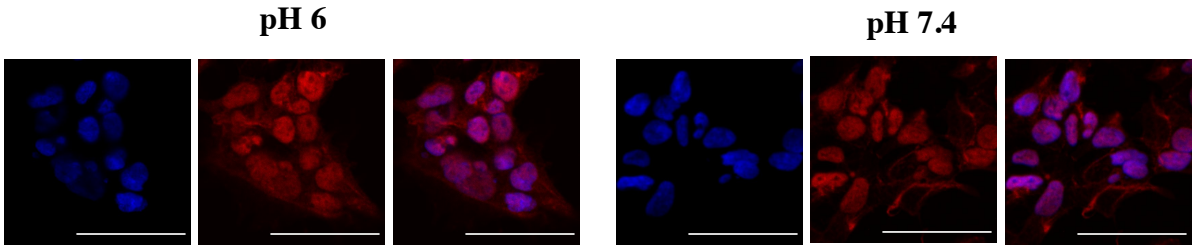

Figure 3. 6 Imaging of HEK cells processed under different conditions using a mouse MeCP2 antibody show an enhanced localization of MeCP2 to the nucleus. HEK cells were fixed with either pH 6.5 (left three columns) or pH 7.4 PFA (right three columns). After fixation, HEK cells were stained with 1:10,000 mouse anti-MeCP2 antibody (M6818, Sigma-Aldrich). In this figure, only the non-blocked images are shown as no difference was observed when blocking was performed. Blue = DAPI, Red = MeCP2. Scale bars represent 50 μm.

Therefore, the final conditions used to stain ReNCell were to use the pH 7.4 PFA fixation, without blocking and with a dilution for the mouse MeCP2 antibody (M6818, Sigma-Aldrich) at 1:10,000. Unfortunately, this condition failed to visualize proper nuclear localization

of MeCP2 in ReNCell for reasons that could not be understood (Fig. 3. 7). A large amount of extranuclear binding and almost complete absence from the nucleus were observed.

The same pattern was observed with the MeCP2 deficient ReNCell indicating that the MeCP2 antibody binding was completely unspecific (Fig. 3. 8).

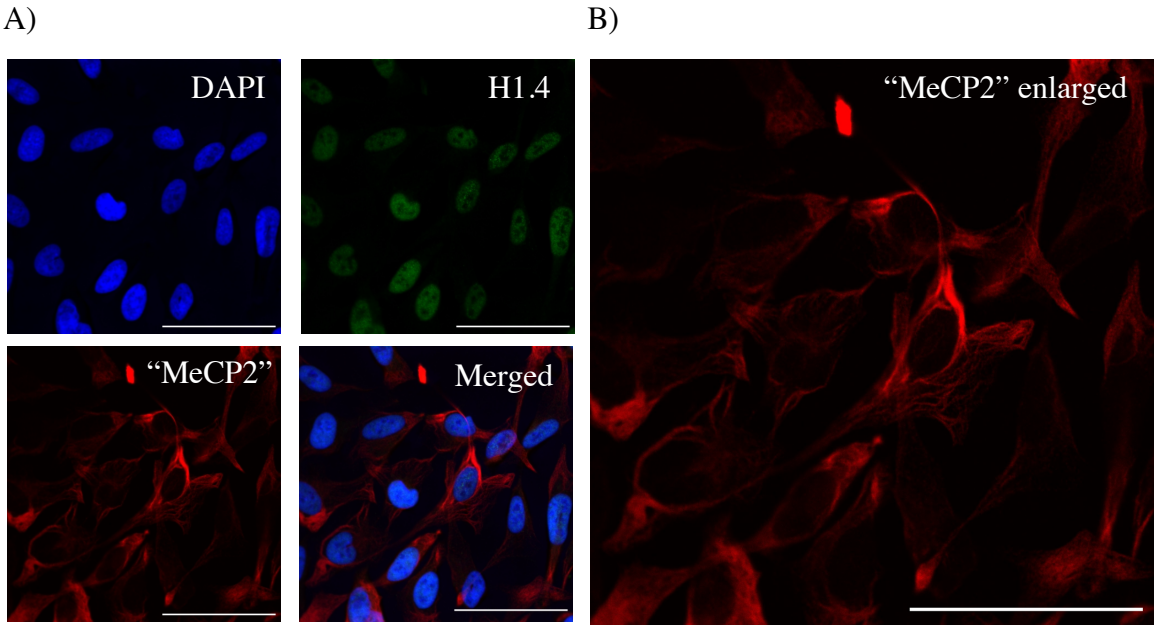

Figure 3. 7 The optimized conditions for MeCP2 visualization fails to localize MeCP2 to the nucleus in WT ReNCell at 0 DIV. A) ReNCells were fixed with pH 7.4 PFA, not blocked and stained with DAPI, 1:500 rabbit H1.4 (41328S, CST) antibody and 1:10,000 mouse MeCP2 antibody (M6818, Sigma-Aldrich). **B)** Enlarged image of "MeCP2" shown in A). Scale bars represent 50 μm.

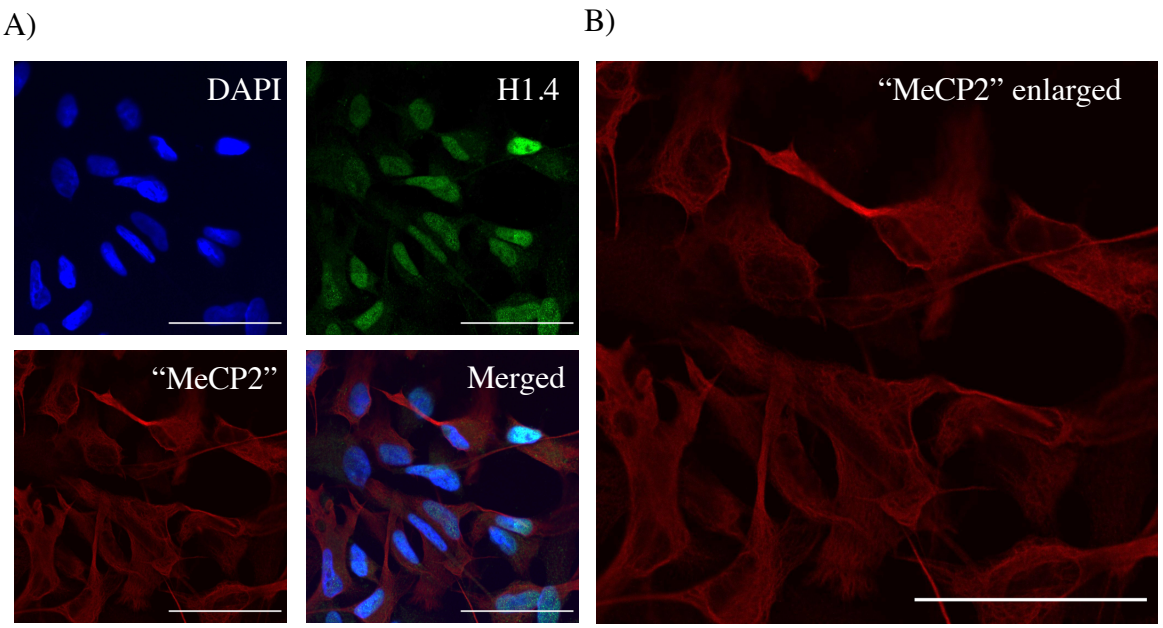

Figure 3. 8 MeCP2 antibody used has unspecific binding as it could be seen in MeCP2 deficient ReNCell at 8 DIV. A) ReNCells were fixed with pH 7.4 PFA, not blocked and stained with DAPI, 1:500 rabbit H1.4 (41328S, CST) antibody and 1:10**,**000 mouse MeCP2 antibody (M6818, Sigma-Aldrich). B) Enlarged image of "MeCP2" shown in A**)**. Scale bars represent 50 µm.

3.3 Immunofluorescence imaging of histone H1.4

While performing different IF visualizations, a pattern of stronger H1.4 staining in WT 8 DIV cells compared to KO 8 DIV cells was systematically observed (Fig. 3. 9 and 10). However, accurate quantification of intensity for immunofluorescence proved difficult because of differences in the exposure settings used for different samples. Regardless, quantification was not the scope of the immunofluorescence imaging used here. A noticeable distinct punctuated pattern of H1.4 distribution in WT 8 DIV different from KO cells and WT at 0 DIV could be observed (Fig. 3. 10; Appendix C and D). In all other cells except WT 8 DIV, there are larger, circular foci seemingly depleted of or with lower levels of H1.4 (Fig. 3. 10; white arrows pointing to foci in WT 0 DIV).

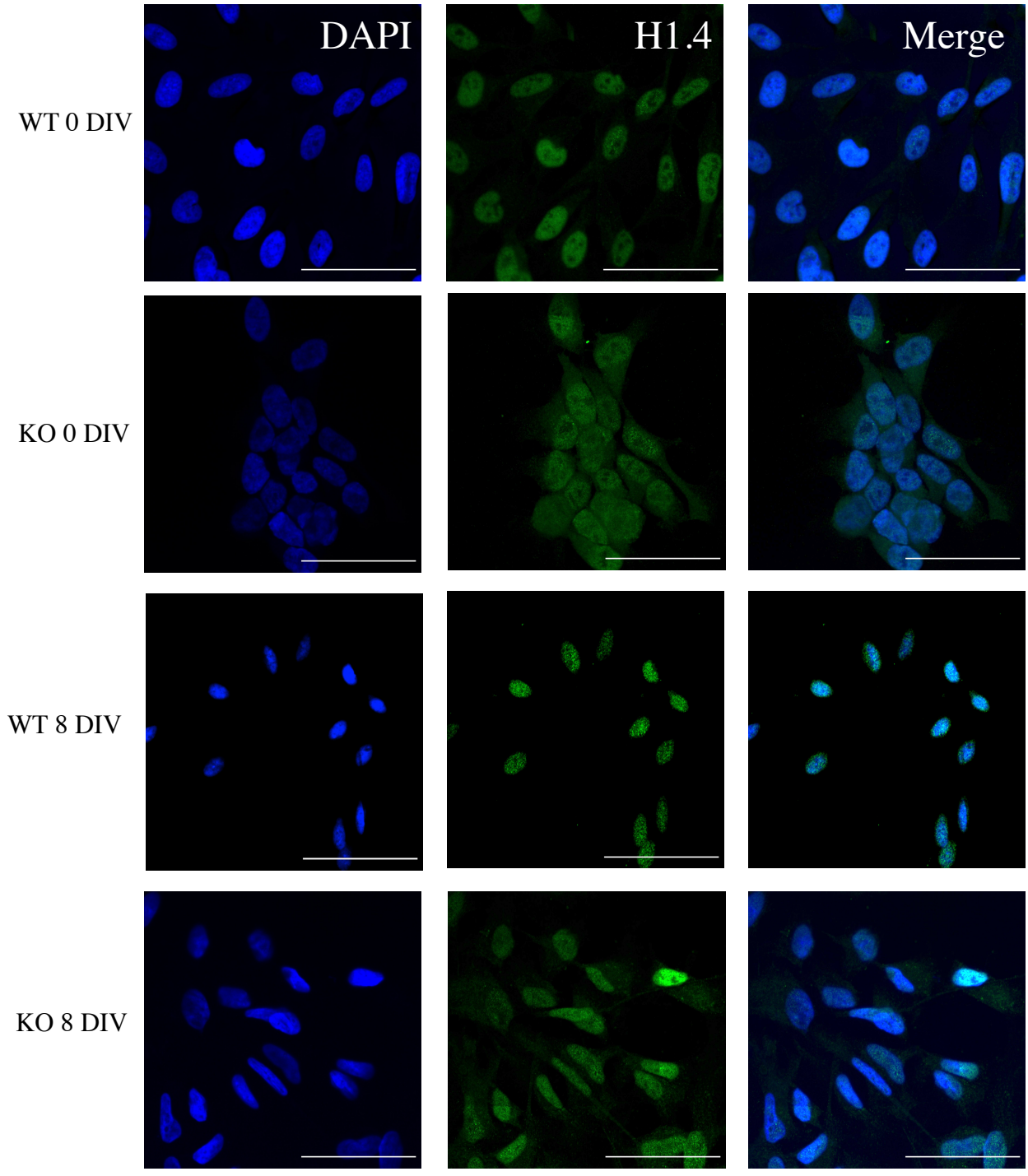

Figure 3. 9 Histone H1.4 imaging in ReNCell WT and KO at 0 AND 8 DIV. Cells were imaged with DAPI (blue) and a rabbit H1.4 antibody (green; 41328S, CST). Scale bars represent 50 μm**.**

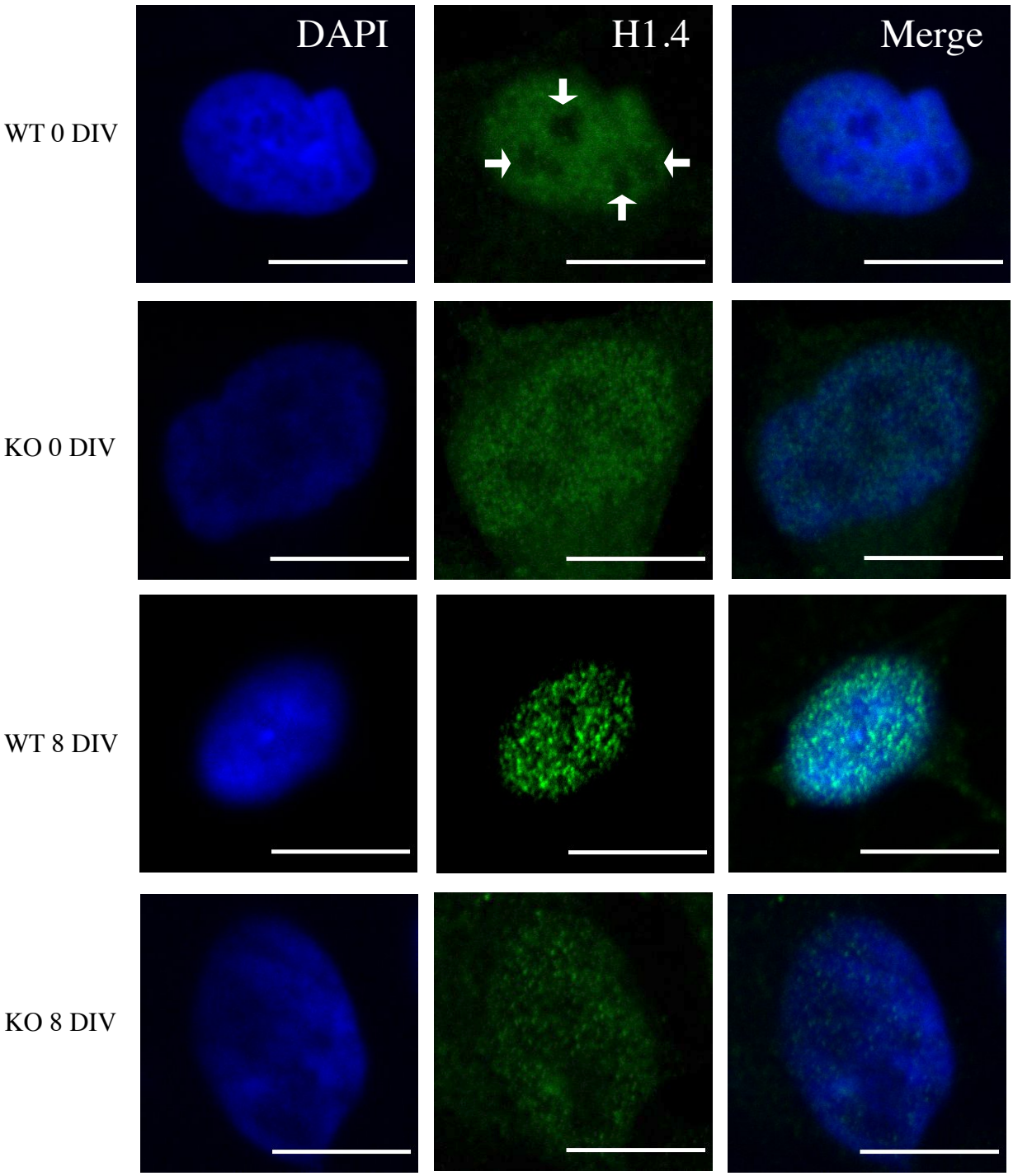

Figure 3. 10 Histone H1.4 has a different nuclear localization profile in ReNCell WT 8 DIV. Cells were imaged with DAPI (blue) and a rabbit H1.4 antibody (41328S, CST) (green). Scale bars represent 10 μm. White arrows in WT 0 DIV, H1.4 point to the foci.

3.4 Change in the nuclear size of MeCP2-KO ReNCell during differentiation

Close-up images of nuclei led to an observation of noticeable differences in their areas for the different ReNCell samples studied. To investigate this further, several areas of nuclei were measured for each cell type and an average was obtained using ImageJ (Fig. 3. 11). The nuclear area of WT ReNCell decreased during differentiation while that of MeCP2-KO ReNCell increased (Fig. 3. 11). The comparison of WT and KO cells at each DIV also showed significant differences where at 0 DIV, WT cells had significantly higher nuclear area than the KO counterpart, while the opposite was observed at 8 DIV (Fig. 3. 11).

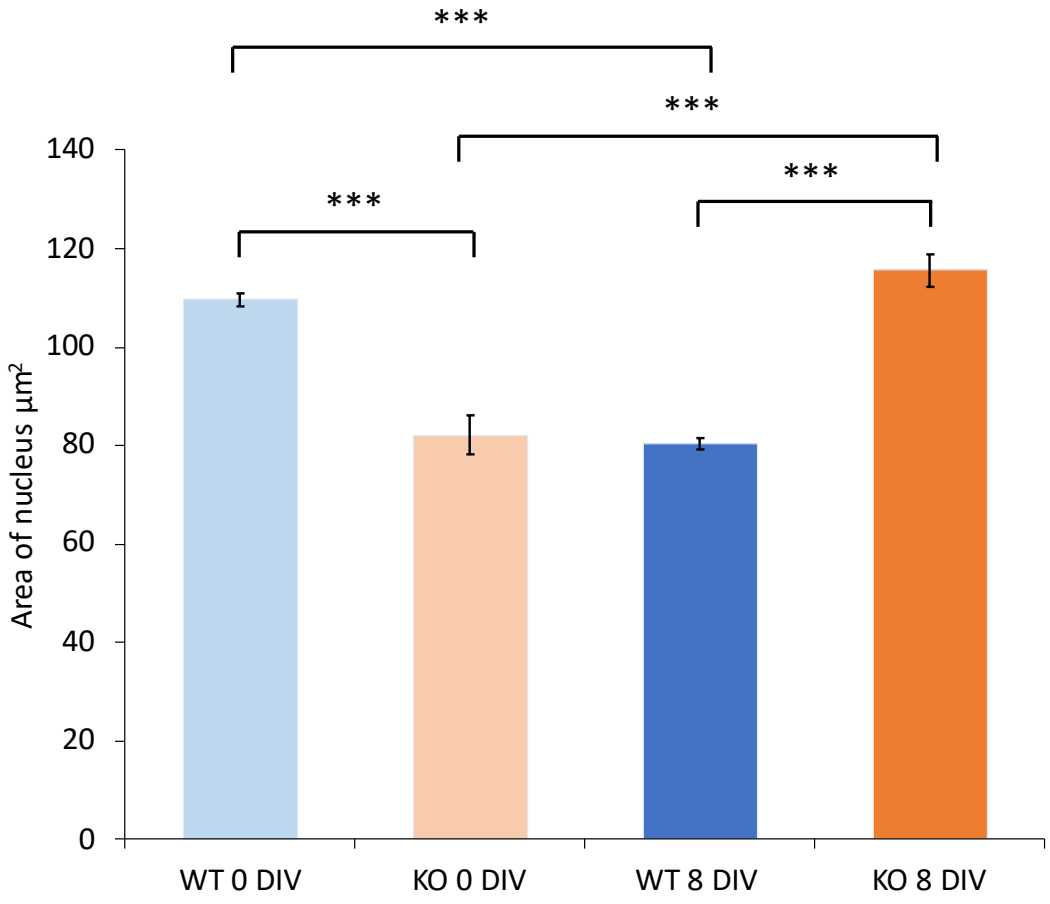

Figure 3. 11 At 8 DIV, KO ReNCell has a higher nuclear area compared to the WT counterpart while at 0 DIV, KO ReNCell has a smaller nuclear area compared to the WT. (n = 570 for WT 0; n = 59 for KO 0; n = 285 for WT 8; n = 105 for KO 8. Two sample t-test assuming unequal variances, $p < 0.0001$ for all comparisons).

Chapter 4. Discussion

Whole mouse brains show an increase of MeCP2 and histone H1.0 but no significant changes in histone H1.4

As a preamble to the studies described in this thesis, a quantitative western analysis of MeCP2 and histones H1.0 and H1.4 in whole mouse brains was performed. MeCP2 is a highly abundant protein in neurons and it increases during neuronal development (Fig. 1. 6)[38]. Histone H1.0 is a H1 subtype that often increases in differentiating neurons (Fig. 1. 6) and cell types with decreased rate of proliferation[13,81]. Despite the cell heterogeneity of this tissue with diverse cell types that do not necessarily exhibit the same increase of MeCP2[82], it was possible to observe an increase of this protein (Fig. 2. 1). Olson et al. (2014) used whole brain tissue and observed similar results[71]. Though in 2004, Kishi and Macklis showed that MeCP2 is expressed in neuronal cells but not in glial cells[38], it was found in 2009 that MeCP2 is expressed in glia, albeit at lower levels than in neurons[82]. In the case of histone H1.0, the increase observed in whole brain (Fig. 2. 2A) is not surprising as both neurons and glia accumulate H1.0 during development[13].

The developmental analysis of the histone H1.4 subtype using whole brain was aimed to replicate the observations of Pearson *et al*. (1984) which showed that the global level of histone H1 decreased by half during cortical neuron development[51]. Similarly, Skene *et al*. (2010) had shown that cortical neurons purified from MeCP2-KO mouse brain had double the normal level of histone H1. Therefore, it was hypothesized whole brains would show a decrease of histone H1.4 during development and that MeCP2-KO mouse brains would have double the level of histone H1.4 compared to the WT counterpart. However, the results obtained in this instance (Fig. 2. 4) were inconclusive and no change could be observed most likely because in the whole brain the

change in H1.4 is lot more subtle than the that of MeCP2 and H1.0. Because of the subtlety, the change in H1.4 in neurons may be masked by other cell types. This was implied in Skene et al. (2010) where the comparison of unsorted cells (combination of neurons and glia) between WT and MeCP2-KO mouse brain showed no difference in the total histone H1 level. Moreover, the H1.4 antibody did not exhibit the quality required for quantitative western blot analysis as described next.

Histone H1.4 could not be quantified by quantitative western blot analysis in ReNCell

ReNCell was used next to try to quantify H1.4 to try to circumvent the masking introduced by the brain tissue and cell heterogeneity. ReNCell is a neural progenitor cell model which can be differentiated into neurons and therefore provide a less heterogenous sample than whole brain. Many of the publications regarding MeCP2 and histone H1 use purified neurons[53] so using ReNCell would be one step closer to using purified neurons. Moreover, ReNCell that is MeCP2 deficient was also available. With WT and MeCP2-KO ReNCell, it was expected that the change in the levels of histone H1.4 which could not be observed in whole brain would be observed. Unfortunately, producing consistent technical replicates for H1.4 continued to prove difficult. A big contributing factor of robust quantitative western data is the quality of the antibody. The failure to produce good technical replicates was most likely due to the unreliability of the H1.4 antibody because western blots with the same samples using the same blotting conditions but with different antibodies (MeCP2 and NeuN) produced reproducible technical replicates (Fig. 2. 3A and Fig. 2. 5).

ReNCell does not express detectable levels of histone H1.0

Histone H1.0 is a subtype which increases in cells which undergo terminal differentiation in many cell types including neurons and glia[13,50,75]. It was thus predicted that when ReNCell is induced to differentiate, the cells would accumulate H1.0 as differentiation proceeded. However, even after differentiation for 24 days in both the WT and KO, no H1.0 could be detected (Fig. 2. 4). It is possible that ReNCell, because it is an immortalized cell line, does not undergo proper terminal differentiation and hence it lacks histone H1.0. Also, it has been reported that some types of neurons lack H1.0[83]. ReNCell originates from the ventral mesencephalon where there is an abundance of dopaminergic neurons, and it is possible that these neurons do not express H1.0. Histone H1.0 is not an essential histone; mice can develop normally without H1.0, and there are no developmental or anatomical anomalies observed when H1.0 is knocked out[84]. Fan *et al*. (2001) showed similar results of no developmental issues when H1.0 was knocked out. This was attributed to other histone H1 subtypes compensating for the loss of H1.0[85]. In fact, Ponte *et al*. (1994) describe that although the CNS contains many different terminally differentiated cells and therefore a large amount of H1.0, terminal differentiation is not a sufficient condition for H1.0 expression as there are some neurons such as Purkinje neurons in the cerebellar cortex that do not express H1.0[83]. Although this paper was based on observations using mouse tissues rather than in humans and does not make any mention to dopaminergic neurons, it is possible that ReNCell lacks H1.0. This result is consistent with the RT-qPCR results showing that H1.0 expression is the lowest compared to the other 2 subtypes, H1.2 and H1.4 (Fig. 2. 12).

Although statistically inconclusive, the data suggest some histone H1 dysregulation in the absence of MeCP2

Given the difficulties encountered with the quantitative western blots, attention was shifted towards the quantification of the total amounts of histone H1 using HPLC and Coomassie-stained SDS-PAGE. Both SDS-PAGE and HPLC were successful at separating all the histones and hence, I was able to quantify histone H1 proteins using these two techniques. Coomassie-stained gel analysis takes into account the binding efficiency of the Coomassie dye to each protein, which depends on the amino-acid composition of the protein. As linker histones are rich in lysine and core histones, in arginine, the relative binding of Coomassie to these two proteins will differ (Appendix B). In HPLC, the different areas of the eluting peaks is based on the absorbance at 230 nm and linker histones would have a different extinction coefficient than core histones[2]. Therefore, the H1 ratios shown in Figs. 2. 9A and B do not correspond to molecular ratios. Despite these considerations, quantification via HPLC and Coomassie staining of gels are in good agreement and provided a way of estimating the overall amount of total histone H1 relative to core histones which appears to change little regardless of the presence of MeCP2 or the DIV time (Fig. 2. 9). However, even though not statistically significant, both Figure 2. 9A and B show a visible increase in histone H1 in MeCP2 deficient ReNCell that has been differentiated for 8 days.

Using RT-qPCR with subtype-specific histone H1 primers showed that there was again no statistically significant difference in the subtype transcript levels regardless of the presence of MeCP2 or the degree of differentiation. However, Figure 2. 10 showed a decreasing trend for all three histone H1 subtypes in proliferating KO ReN cells. Urdinguio *et al*. (2008) showed that when MeCP2 was knocked out, there were several overexpressed transcripts in the different parts

of the brain: cortex, midbrain and cerebellum[86]; however, histone H1 was not one of those transcripts. The RT-qPCR results are in accordance with this.

In summary, HPLC was a good method to separate and ascertain the histone H1 stoichiometry while RT-qPCR was a good method of quantification of the subtypes' transcripts. These results show that in ReNCell, despite the statistically insignificant small changes observed, these changes suggest a potential involvement of MeCP2 in the regulation of histone H1 content and expression.

Linker histones in ReNCell WT and KO are eluted differently in HPLC

An observation from the western blots of the different HPLC fractions collected was that histones H1.2 and H1.4 eluted differently in MeCP2-KO ReNCell compared to WT ReNCell (Fig. 2. 8B). RP-HPLC separates molecules depending on their different chemical composition, mainly based on their hydrophilicity. This result is interesting as it suggests that despite no big differences in the levels of the histone H1 subtypes, their elution patterns might be affected by some different PTMs depending on the presence or absence of MeCP2. Wisniewski et al. (2007) confirmed that the presence of PTMs affected the retention on the column for histone H1 proteins in RP-HPLC[26]. One of the most prominent PTM on histone H1s is phosphorylation. Histone H1 subtypes are well known to change their phosphorylation depending on the stage of the cell cycle[24]. As the immunofluorescence results show, the lack of MeCP2 yields a different morphology of ReNCell at 8 DIV which may suggest a lack of proper differentiation. A consequence of this may be the occurrence of altered PTM on the histone H1 complement which might be responsible for the different elution pattern observed by the RP-HPLC results. Future MS analysis may provide additional information to this observation as I note in "Importance of Results and Future Directions."

Histone H1.4 is the most abundantly transcribed histone H1 subtype

In all ReNCell samples analyzed, H1.4 was the most abundant histone H1 transcript (Fig. 2. 12 and Appendix E). These results are in agreement with the results of Dominguez et al. (1992) describing that H1.4 becomes the dominant histone H1 subtype in rat cortical neurons during postnatal development[75]. The second most abundant histone H1 subtype in ReNCell was H1.2. It is notable how in different publications, H1.2 and H1.4 seem to be closely associated. In a study carried out with a human neutrophil-like cell line, PLB-985, the authors found that loss of H1.2 and H1.4 prevented the cells from maturing[87]. Also, in T47D cells, the absence of H1.2 causes cell cycle arrest at G1 phase while the absence of H1.4 causes cell death[18]. Finally, H1.2 and H1.4 are the two histone H1 subtypes that are almost always present in many cell lines (and tissues) examined[19]. These results show that choosing H1.2 and H1.4 for the analysis carried out here was a good choice as these two H1 subtypes are often the most prominent subtypes.

ReNCell MeCP2-KO cells are unable to differentiate properly and aggregate in culture

The immunofluorescence images of WT and KO ReN cells showed major differences in their morphology especially at 8 DIV (Figs. 3. 1 and 3. 2). The images show that WT cells are more advanced in their differentiation as seen by long projections and connections between cells (Fig. 3. 2). On the other hand, after differentiation for 8 days, MeCP2 deficient ReN cells showed fewer projections and more lamellipodia indicative of a stage where cells are less differentiated and/or attempting to differentiate.

Another observation is the aggregation of MeCP2-KO ReN cells (Figs. 3. 1 and 3. 2). In this regard, the early observations by Armstrong *et al.,* (1995) on RTT neuron morphology provide a possible explanation for this, assuming that MeCP2-KO ReN cells mimic the RTT phenotypes observed in MeCP2-KO mice. A decrease in the number and length of dendrites as

well as more dense packing of neurons were described[88]. The absence of MeCP2 may cause MeCP2-KO ReN cells to stay close together as opposed to the WT cells where cells have proper neurite outgrowths and are spaced out. Chen *et al*. (2001) also observed that deletion of MeCP2 within the CNS led to neurons being more densely packed[47], which is also consistent with my results on MeCP2-KO ReNCell.

In summary, immunofluorescence images show that when MeCP2 is knocked out, proper cell differentiation in ReNCell is impaired. This provides an important consideration for the interpretation of the results obtained in other aspects of the current project. The lack of a difference in the levels of total histone H1 proteins between WT and MeCP2-KO ReNCell may be because of the difference in the progression of differentiation between the two cell lines rather than a direct consequence of the physical presence or absence of MeCP2 in these cell types.

Histone H1.4 exhibits a distinct chromatin localization in WT ReNCell at 8 DIV

To analyze how the effects described in the previous section impact H1.4 localization in the nucleus, it was of interest to look at how H1.4 localization would differ in the presence or absence of MeCP2. Unfortunately, it was not possible to visualize MeCP2.

Regardless, this unanticipated problem did not divert the main objective regarding the H1.4 localization in the presence or the absence of MeCP2. WT ReNCell that was differentiated for 8 days had a punctuated nuclear distribution of H1.4 that was different from other cells. This contrasts with WT and KO ReNCells at 0 DIV which exhibit a diffuse chromatin distribution of H1.4 throughout the nuclei. After 8 days in differentiation of MeCP2 deficient ReNCells, a somehow incipient punctuated organization appears to be more diffuse compared to the corresponding WT cells. This could be due to different chromatin organization which occurs with the proper neuronal differentiation/development which is happening in the presence of

MeCP2. The chromatin organization depicted by H1.4 observed for WT ReN cells differentiated for 8 days is reminiscent of a very similar distribution described in a recent paper for this subtype[63]. The authors of this paper analyzed the different genomic distribution of histone H1 variants H1.0, H1.2, H1.4, H1.5 and H1.X. They found that H1.4 is preferentially enriched in GC rich regions and immunofluorescence analysis carried on a T47D breast cancer cell line for each of these variants exhibited a distinctive nuclear localization with that of H1.4 almost identical to that observed for WT ReNCell at 8 DIV (Fig. 3. 10). Histone H1.4 exhibited a higher presence in the short TADs (topologically associating domains; regions of the chromosome which makes spatial associations internally[89]) of the A (active nuclear) compartment which is characterized by an open chromatin organization (Fig. 1. 5A). An open chromatin conformation is a characteristic of differentiated neurons[90] and hence the similarity is not surprising.

Immunofluorescence images suggest a developmental delay in MeCP2 deficient ReNCell that has been differentiated for 8 days as reflected in the more diffuse distribution of H1.4 in this sample. Fan *et al*. (2005) showed that the mouse ESCs with triple KO of histone H1 subtypes (H1.2, 3 and 4) did not result in different nuclear localization of MeCP2[10]. Hence, the result with histone H1.4 indicates that while MeCP2 may have indirect or direct effect in histone H1 localization, histone H1 may not have a bearing on the MeCP2 localization. However, the dynamics involved may depend on the cell types and context.

MeCP2 deficient ReN cells at 8 DIV displays a higher nuclear area compared to the WT counterpart

An unexpected observation from the immunofluorescence images was that at 8 DIV, MeCP2-KO ReN cells had a significantly higher nuclear area compared to WT ReN cells (Fig. 3. 11). This observation seems to contradict the results of several previous publications. Chen *et al*.

(2001) showed that CNS-specific deletion of MeCP2 led to decreases in both the neuron size and nuclear size in several areas of the brain[47]. These measurements were carried out using neurons in the CA2 region of the hippocampus. Li *et al*. (2013), Stuss *et al*. (2013) and Rietveld *et al*. (2015) also showed that MeCP2 mutant neurons have smaller nuclei compared to WT neurons[56,91,92]. Yazdani *et al*. (2012) obtained similar results using a stem cell-based neuron system where they observed an increase (approximately two-fold) of H1 in the differentiated neurons lacking MeCP2 and speculated that the smaller nuclei of MeCP2-KO neurons is due to the increased level of histone H1[57] as histone H1 has previously shown to be one of the proteins determining nuclear size[58]. Following this logic, the expectation for MeCP2 deficient ReNCell would be that the absence of MeCP2 should lead to an increase of histone H1 which would result in a smaller nuclear size of these cells. However, the results of Figure 2. 9 show that although the histone H1 content is not statistically different between WT and MeCP2-KO ReNCell, the results comparing the two cell types show a trend of a slight but noticeable increase of H1 in the latter. In this regard, it is important to consider here that there is also no difference in the level of histone H1 between 0 DIV and 8 DIV for WT ReNCell. The lack of significance observed in both instances may be due to the fact that the increase observed in Figure 2. 3A for MeCP2 in WT ReNCell during differentiation never reaches the values observed in native neurons during differentiation. The increase observed in WT ReNCell at 8 DIV is 5 times lower than that observed in whole mouse brain and approximately 10-times less than in cortical neurons (results not shown). A very similar reduction in the levels of MeCP2 was observed in a previous study when SH-SY5Y, PC-12 and NG 108-15 cell lines were induced to differentiate *in vitro* into neuron-like postmitotic cells[70]. Therefore, a 10% increase in MeCP2 in WT ReN cells differentiated for 8 days would be expected to result only in a small decrease in H1, which would

be difficult to precisely measure by the quantitative western approach used here. Regardless, it is possible that other proteins or mechanisms are involved[93] in the unpredicted increase of the size of neuronal nuclei observed in MeCP2 deficient ReN cells at 8 DIV (Fig. 3. 11).

Factors possibly contributing to histone H1 abundance other than MeCP2.

An early *in vitro* study by Nan *et al*. (1997) showed that MeCP2 can displace histone H1 in a DNA methylation dependent way[54]. Further biophysical and *in situ* experiments using H1.0 constructs provided further support to these early data[30]. In 1984, before MeCP2 had been described, Pearson *et al*. described that cortical neurons contained a low level of histone H1 approximately ½ compared to the 'normal' one H1 molecule/nucleosome ratio[51]. More recently, Skene *et al*. (2010) found that neurons from a mouse MeCP2-KO brain contained double the amount of histone H1 compared to the WT[53]. All of this was taken to indicate that MeCP2 and histone H1 compete for similar chromatin binding sites where the increase in MeCP2 observed during neuronal differentiation (Fig. 2. 1) is responsible for the decrease in H1 observed in mature neurons. However, in 2018, Ito-Ishida et al. performed ChIP-Seq and showed that binding of MeCP2 and histone H1.0 are largely unrelated[68] and hence the mystery of the low levels of histone H1 in neurons still remains.

Despite the elegance of the parsimonious competition hypothesis, there are several other ways by which histone H1 can be regulated in neurons. A possibility for the drop in histone H1 in neurons is the effect of cell cycle. Early studies have shown that in cells blocked in early S phase by 5'-fluorodeoxyuridine or Aphidicolin, the histone H1 level is reduced 20 – 60 %[94]. Also, when Happel *et al*., (2009) arrested the cell cycle of HeLa using sodium butyrate, the expression of H1.1-H1.5 decreased even though these cells have a very low content of MeCP2[95]. Similarly, there is a possibility that as neural progenitor cells are triggered to differentiate, the

expression and protein levels of the replication-dependent somatic linker histone subtypes (H1.1 to H1.5) decrease while the replication-independent histone H1 subtypes (H1.0 and H1.x) increase. Cell cycle arrest is necessary for terminal cell differentiation which means that the consequences of cell cycle arrest should be present in differentiating neurons at their differentiation end point. Something that could impede in ReNCell the full effect of cell cycle arrest and differentiation observed in native neurons could be the incorporation of v-myc gene into ReNCell genome when this cell line was artificially immortalized. Unlike this *in vitro* system, most neurons in the brain are proliferative before birth and shortly after birth, commit to terminal differentiation. In this regard, the artificial immortalization of neural progenitor cells could limit the study of chromatin-associated proteins such as histone H1s. Hence, ReNCell may not be the best model to fully study the MeCP2 and histone H1 interaction.

Many studies done with the aim to decipher the relationship between MeCP2 and histone H1 use cortical neurons and make claims about these proteins as if the observation could be generalized to every type of neuron, something that was questioned in the early paper by Kuenzle[49]. However, there are many different types of neurons in the brain and each type of neuron is very different in terms of morphology and functionality and therefore it would not be surprising if these would exhibit different chromatin arrangements. This might mean that the dynamics and abundance of MeCP2 and histone H1 are different in different types of neurons. This could also be true for ReNCell which originates from the ventral mesencephalon, a region where dopaminergic neurons reside.

Importance of Results and Future Directions

This study is novel as it provides an examination of MeCP2 and histone H1 in ReNCell, a cell type that can be induced to differentiate into neurons but for which there is no information regarding the chromosomal protein composition during the process.

A recent study from 2018 has shown that dopaminergic neurons differentiated from a stem cell isolated from a RTT patient had decreased numbers of neurite outgrowth and branches[96]. The study noted that it is the stunted function of mitochondria in these cells that contribute to the disease. Also, knocking out MeCP2 from dopaminergic neurons leads to problems in motor coordination[97]. All these results point to the relevance of working with dopaminergic neurons as it pertains to RTT studies. In this regard, ReNCell and a similar cell line LUHMES both derived from the ventral mesencephalon, a region highly enriched in dopaminergic neurons and for which there is a MeCP2-KO cell line may be also very pertinent[98]. Using these *in vitro* systems could be used to study the neuronal malfunction caused by MeCP2 deficiency.

There are also studies which show that MeCP2-KO astrocytes or other glial cells have negative non-cell-autonomous effects on neurons[99,100]. Looking at various cell types in the brain for MeCP2 and branching out to other organelles beyond the nucleus may provide more information on the biology of the protein itself and the etiology of RTT.

Although MeCP2 and histone H1 are abundant chromosomal proteins in neurons, these are not the only chromatin associated proteins. HMGs for example have been implicated in neuronal development[101], and they have been shown to compete with histone H1[102,103]. Studying other chromatin associated proteins would shed more light on the general chromatin arrangement and the diverse processes that all these proteins are involved in.

For this work, specifically for HPLC, the HCl-extracted histones were used in order to obtain both core and linker histones as core histones were required to normalize the levels of linker histones. In future qualitative studies on histone H1, 5% PCA (perchloric acid) could be used to extract linker histones specifically (Fig. 4. 1). With such extracts, it should be possible to perform HPLC and proceed with MS analysis of the histone H1 subtype PTMs.

Currently most of the research on histone PTMs focuses on core histones and several of these PTMs have been associated with defined chromatin functions, such as H3K4me3 and gene activation[104]. Similar research has more recently started to be performed on linker histones in order to elucidate their linker contribution to the histone code[105,106]. For example, H1.4 K34 acetylation at gene promoters is associated with gene activation[107]. Even though HPLC may not provide an ideal method of protein quantification, HPLC proved an effective method to separate the different subtypes. So, with the HPLC fractions, further analysis can be carried out via MS. On this note, it would be good to move away from quantification and move to more qualitative studies in the future. By using MS techniques, it should be possible to analyze the different PTMs that occur on histone H1 subtypes as a direct or indirect effects of the MeCP2 presence or absence.

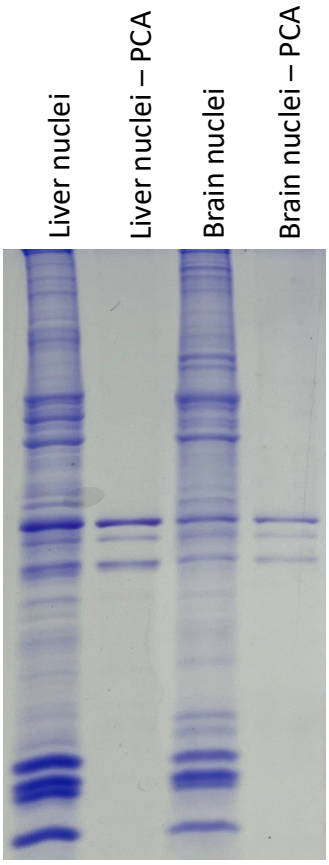

Figure 4. 1 5% perchloric acid can specifically extract linker histones. SDS-PAGE gel of mouse liver and brain nuclei and their corresponding 5% PCA extracts.

Conclusion

This is the first study to date to investigate the relationship between MeCP2 and histone H1 in ReNCell VM neural progenitor cells. The results show that within the approximately 5-fold increase in MeCP2 observed in WT ReNCell induced to differentiate, very small, if any, changes in the amount of histone H1 were observed, compared to what has been published with mouse cortical neurons where the amount of MeCP2 at the peak of differentiation is approximately tenfold higher and the level of histone H1 decreases by half compared to the proliferating, embryonic stage (Fig. 1. 6). However, the different elution patterns of histones H1.2 and H1.4 in HPLC show that the absence of MeCP2 may directly or indirectly result in changes in the PTMs of the histone H1 subtypes, which warrant further studies in the future. Two stark differences caused by the absence of MeCP2 in ReN cells was their altered morphology and the increased size of their nuclei. Results from this work will provide a useful reference for further studies using ReNCell in the context of neural progenitor cells and/or chromatin associated proteins.

Materials and Methods

Catalogue numbers and references for reagents

Reagents for nuclear preparation	
Protease inhibitor	Roche Molecular Biochemicals, Laval, QC, Canada; 5056489001
Antibodies used for western blot	
H1.0	Santa Cruz, Dallas, TX, USA. SC-56695
H1.2	Invitrogen, Waltham, MA, USA. PA532009
H1.4	Invitrogen, Waltham, MA, USA. PA544881
H1.4	Invitrogen, Waltham, MA, USA. 702876
H1.4	Cell Signaling Technologies, Danvers, MA, USA. 41328S
H4	Produced in house
MeCP2	Sigma-Aldrich, St. Louis, MO, USA. M9317
NeuN	Sigma-Aldrich, St. Louis, MO, USA. MAB377
IRDye M680 Anti-mouse	Licor, Lincoln, NE, USA. 926-68070
IRDye 800 Anti-rabbit	Licor, Lincoln, NE, USA. 611-132-122
Antibodies used for immunofluorescence	
MeCP2 (anti-mouse)	Sigma-Aldrich, St. Louis, MO, USA. M6818
MeCP2 (anti-mouse)	Sigma-Aldrich, St. Louis, MO, USA. WH0004204M1
MeCP2 (anti-chicken)	N/A (provided by Dr. Kerry Delaney)
H1.4	Cell Signaling Technologies, Danvers, MA, USA. 41328S
NeuN	Sigma-Aldrich, St. Louis, MO, USA. MAB377
Alexa fluor 488 (Goat anti rabbit IgG H&L)	Abcam, Cambridge, UK. Ab150077
Alexa fluor 568 (Goat anti mouse IgG H&L)	Abcam, Cambridge, UK. ab175473
Reagents used for immunofluorescence	
16% PFA	Electron Microscopy Sciences (EMS), Hatfield, PA, USA. 15710

Coverslips	Bellco Glass Inc., Vineland, NJ, USA. 50-194-4702
Horse serum	Gibco, Waltham, MA, USA. 16050130
Immumount	Thermo Shandon Limited, Cheshire, UK. 9990402
SGC5	Biotium, Fremont, CA, USA. 70057
Cell culture reagents for ReNCell	
DMEM F-12	Sigma-Aldrich, St. Louis, MO, USA. D8437
Antibiotic/antimycotic	Sigma-Aldrich, St. Louis, MO, USA. A5955
B27	Gibco, Waltham, MA, USA. 17504044
Heparin	Stemcell technologies, Vancouver, BC, Canada. 07980
Laminin	Sigma Aldrich, St. Louis, MO, USA. L2020
EGF (epidermal growth factor)	Stemcell technologies, Vancouver, BC, Canada. 78006
bFGF (basic fibroblast growth factor)	Stemcell technologies, Vancouver, BC, Canada, 78003
Accutase	Sigma-Aldrich, St. Louis, MO, USA. SCR005
Reagents for reverse transcription/qPCR	
High Capacity cDNA reverse transcription kit	Applied Biosystems, Waltham, MA, USA. 4368814
SYBR Select Master Mix	Applied Biosystems, Waltham, MA, USA. 4472903
Trizol	Invitrogen, Waltham, MA, USA. 15596026
TURBO DNase	Invitrogen, Waltham, MA, USA. AM2238
Reagents for HPLC	
C_{18} column	Vydac, Hesperia, CA, USA. 218TP54

Cell culture

ReNCell VM cells (both WT and MeCP2-KO) were kindly provided by the Manel Esteller lab in Barcelona, Catalonia, Spain. Both WT and KO ReNCell were maintained in complete media: DMEM/F-12, B27 (1X), antibiotic/antimycotic and heparin with EGF and bFGF. Before ReNCell

was plated, the culture vessel was coated with laminin by incubating the plate surface in 20 mg/mL in PBS for 2 hours at 37 ºC. To thaw ReNCell, the frozen stock was diluted in incomplete media and spun down at 1,000 x g for 3 minutes and the supernatant was removed. The cell pellet was diluted in complete media and plated on the laminin-coated culture vessel. For the induction of differentiation, the cells were briefly washed with DMEM/F-12 and given incomplete media: complete media without growth factors (EGF and bFGF). Days *in vitro* (DIV) notes the number of days after differentiation is induced. Media was changed after the day after subculturing and every other day afterwards.

Nuclear preparation for tissues

Tissues were homogenized in 4 volumes of lysis buffer, "Buffer A" (0.25 M Sucrose, 60 mM KCl, 15 mM NaCl, 10 mM MES (pH 6.5), 5 mM $MgCl_2$, 1 mM $CaCl_2$, 0.5% triton X-100) with 1:100 protease inhibitor. The homogenate was incubated on ice for 10 minutes and centrifuged at 600 x g for 5 minutes at 4 ºC. The pellet was resuspended in 8 volumes of Buffer A and centrifuged at 600 x g for 5 minutes at 4ºC. The pellet was resuspended next in 4 volumes of nuclei wash buffer "Buffer B" (50 mM NaCl, 10 mM Pipes (pH 6.8), 5 mM $MgCl_2$, 1 mM $CaCl_2$) and centrifuged. The pellet thus obtained resuspended in 2 volumes of Buffer B. For measuring the concentration of DNA, 5 μL of sample in buffer B was added to 975 μL of distilled water to lyse the nuclei, vortexed, then 20 μL of 10% SDS (final concentration of 0.2% SDS) was added and the absorbance at 260 nm was measured using CARY 1 BIO UV-Vis Spectrophotometer. An extinction coefficient A_{260} of DNA = 20 cm^2mg^{-1} was used[108].

Nuclear preparation of ReNCell for subsequent HCl extraction

To harvest the cells, Accutase was added to ReNCell and incubated at 37 ºC for 5 minutes. The detached cells suspended in Accutase solution were transferred to a centrifuge tube and centrifuged at 1,000 x g for 3 minutes at 4 ºC. The pellet thus obtained was resuspended in 2 volumes of buffer A. Then the suspension was centrifuged at 600 x g for 5 minutes at 4 ºC. The supernatant was removed, and the pellet was frozen at -80 ºC for 2 hours. The frozen pellet was subsequently used for HCl extraction.

HCl extraction of histones

Nuclei suspended in buffer A or B was mixed with 6 volumes of 0.8 N HCl and homogenized. Homogenate was centrifuged at 13,000 x g for 10 minutes at 4 ºC and 6 volumes of acetone were added to the HCl supernatant. The mixture was incubated overnight at -20 ºC to precipitate the histones. The next day, the mixture was centrifuged at 13,000 x g for 10 minutes 4 ºC. The acetone supernatant was removed, and the pellet was washed in fresh acetone. The pellet does not resuspend well in the acetone, so the pellet was dispersed with a thin spatula in the freshly added acetone at room temperature. Then the mixture was centrifuged again as per the previous steps' conditions. The final acetone supernatant was removed, and the pellet was vacuum centrifuged on Jouan RC 1010 concentrator centrifuge for 10 minutes at room temperature. The dry pellet was dissolved in distilled water and mixed with 2X SDS for running in a gel or had its absorbance measured at 230 nm using Nanodrop™ (NanoDrop Technologies Inc, Wilmington, DE, USA).

SDS-PAGE

Cell or nuclear lysates were mixed with 2X Laemmli buffer (2% SDS, 10% glycerol, 0.002% bromophenol blue and 62.5 mM Tris-HCl pH 6.8) and run on an SDS gel (15% separating, 4% stacking). SDS-PAGE was performed as previously described[109]. The gel was run in buffer (0.38 M glycine, 0.05 M tris-base, 0.1% SDS). For staining, the gel was incubated in Coomassie staining solution (10% acetic acid, 0.27% Coomassie Brilliant Blue G-250, 25% isopropanol) for one hour at room temperature on shaking. The gel was then placed in de-stain solution (10% isopropanol, 10% acetic acid) for one hour at room temperature on shaking.

Western blot (for Western section)

The proteins were transferred using sodium phosphate transfer buffer (20 mM $NaPO_4$, 15% ethanol and 10 mL of 10% SDS added directly to transfer container after blotting set up is complete) to nitrocellulose membrane for 2 hours at 400 mA at 4 ºC. The membrane was blocked in 3% blocking buffer (3% skim milk powder in PBST; 0.1% tween-20 in 1X PBS) for 1 hour. The membrane was incubated with primary antibody overnight at 4 ºC while shaking. The membrane was then washed three times with PBST then incubated with secondary antibody for 1 hour at room temperature in dark. Membranes were imaged and protein bands were analyzed using Li-Cor Odyssey Clx (LI-COR Biosciences, Lincoln, NE, USA).

RNA extraction, cDNA synthesis, qPCR

Total RNA was extracted using Trizol. Cells were harvested from the plate using Trizol. RNA extraction was carried out according to the manufacturer's instructions. One ug of extracted RNA was reverse-transcribed with High-Capacity cDNA Reverse Transcription Kit according to the

manufacturer's instructions. qPCR was done using Stratagene MX3005P qPCR system (Santa Clara, CA, USA) and MXPro software. Each qPCR reaction consisted of 1X SYBR Select Master Mix, 0.5 μM forward primer, 0.5 μM reverse primer, nuclease free water and 1 μL of appropriately diluted cDNA. Each sample was run in triplicate. Data were analyzed using the Pfaffl method. Neither the no template control (NTC) nor the no reverse transcriptase control (NRT) showed amplification which is an indication that there was no contaminant in any of the reactions and there was no gDNA contamination. Primer pairs used for qPCR are shown below.

Gene – forward/reverse	Primer sequence (5' → 3')
GAPDH - forward	ATGACCACAGTCCATGCCATC
GAPDH - reverse	CCAGTGAGCTTCCCGTTCA
Histone H1.0 - forward	CTCGCAGATCAAGTTGTCCA
Histone H1.0 - reverse	GAAGGCCACTGACTTCTTGG
Histone H1.2 - forward	ACACCGAAGAAAGCGAAGAA
Histone H1.2 - reverse	GCTTGACAACCTTGGGCTTA
Histone H1.4 - forward	GTCGGGTTCCTTCAAACTCA
Histone H1.4 - reverse	GCCTTCTTTGGGGTCTTCTT
RPLP0 - forward	TGTGGGAGCAGACAATGTGG
RPLP0 - reverse	CCGGATATGAGGCAGCAGT

Note:

Human histone H1 transcript primers obtained from[110]
RPLP0 primer sequences obtained from[111]
RPLP0 = ribosomal protein lateral stalk subunit P0
GAPDH = glyceraldehyde-3-phosphate dehydrogenase

HPLC

The HCL-extracts from ReNCell were reconstituted in 1mL of distilled water at an approximate OD_{230} of 0.34 and filtered using a 0.45 μm Nanosep centrifugal filter. Filtrate was injected onto a C18 column (Vydac, 4.6 x 250 mm, particle size: 5 μm, pore size: 300 Å) and eluted at 1 mL/min using mobile phase A (0.1% trifluoroacetic acid in ddH_2O) and mobile phase B (100% acetonitrile).

The program uses a gradient of 0 – 60% (1%/1 mL/minute) of solvent B over 60 minutes. HPLC-separation of proteins was performed on Beckman Coulter SYSTEM GOLD® 126 Solvent Module equipped with SYSTEM GOLD® 168 Detector. The effluent from the HPLC column was monitored at 230 nm and the elution peaks were recorded. Peak areas were determined with the 32 Karat software peak integrator program (Beckman Coulter Inc., Brea, CA, USA). HPLC fractions (1 mL) were collected and were then lyophilized overnight. The lyophilizate was than mixed with a small volume (~20 μL) of 1X SDS on SDS-PAGE gel and analyzed after Coomassie staining or western blotting.

ReNCell culture on coverslips and Immunofluorescence

For immunofluorescence, ReNCell was cultured on 12 mm #1 coverslips. Before ReNCell was plated, coverslips were coated with laminin by incubating the coverslips in 20 mg/mL in PBS for 2 hours at 37 ºC. ReNCell was then cultured in the same way as described above. At defined DIV times, media was removed, and the cells were fixed using ice-cold PFA (4% and pH 7.4 except for the optimizations using different pH). The cells were fixed for 15 minutes on ice. PFA was removed and coverslips were washed with PBS 3 times for 5 minutes each. The cells were permeabilized for 1 hour using 0.4% Triton in PBS at room temperature. They were then washed 3 times for 5 minutes each with PBS. Next, the antibody dilution (diluted in PBS) was put on the coverslips and incubated overnight at 4 ºC. The following day, the antibody was removed, and coverslips were washed with PBS 3 times for 5 minutes each. Secondary antibody dilution (diluted in PBS) was put on and incubated for 1 hour at room temperature in a dark chamber. After removal of the secondary antibody, the coverslips were incubated with DAPI for 10 minutes in the dark. Finally, the coverslips were washed with PBS 3 times for 5 minutes each. Coverslips were mounted

face-down on a glass slide using Immumount as mounting medium and imaged using the Nikon C2 confocal microscope (Nikon, Tokyo, Japan) with a numerical aperture of 1.3. Images were processed using the ImageJ software.

References

1. Luger, K., Mäder, A. W., Richmond, R. K., Sargent, D. F. & Richmond, T. J. Crystal structure of the nucleosome core particle at 2.8 Å resolution. *Nature* **389**, 251–260 (1997).
2. van Holde, K. E. *Chromatin*. (Springer-Verlag, 1989).
3. Simpson, R. T. Structure of the Chromatosome, a Chromatin Particle Containing 160 Base Pairs of DNA and All the Histones. 5524–5531 (1978).
4. Hartman, P. G., Chapman, G. E., Moss, T., Bradbury, E. M. Studies on the Role and Mode of Operation of the Very-Lysine-Rich Histone H1 in Eukaryote Chromatin The Three Structural Regions of the Histone H1 Molecule. *Eur. J. Biochem.* **77**, 45–51 (1977).
5. Widom, J. Chromatin structure: Linking structure to function with histone H1. *Curr. Biol.* **8**, 788–791 (1998).
6. Horowitz, R. A., Agard, D. A., Sedat, J. W. & Woodcock, C. L. The three-dimensional architecture of chromatin in situ: Electron tomography reveals fibers composed of a continuously variable zig-zag nucleosomal ribbon. *J. Cell Biol.* **125**, 1–10 (1994).
7. Lu, X. *et al*. Linker histone H1 is essential for Drosophila development, the establishment of pericentric heterochromatin, and a normal polytene chromosome structure. *Genes Dev.* **23**, 452–465 (2009).
8. Shimamura, A., Sapp, M., Rodriguez-Campos, A. & Worcel, A. Histone H1 represses transcription from minichromosomes assembled in vitro. *Mol. Cell. Biol.* **9**, 5573–5584 (1989).
9. Braunschweig, U., Hogan, G. J., Pagie, L. & Van Steensel, B. Histone H1 binding is inhibited by histone variant H3.3. *EMBO J.* **28**, 3635–3645 (2009).
10. Fan, Y. *et al*. Histone H1 depletion in mammals alters global chromatin structure but causes specific changes in gene regulation. *Cell* **123**, 1199–1212 (2005).
11. Ushinsky, S. C. *et al*. Histone H1 in Saccharomyces cerevisiae. *Yeast* **13**, 151–161 (1997).
12. Wu, M., Allis, C. D., Richman, R., Cook, R. G. & Gorovsky, M. A. An intervening sequence in an unusual histone H1 gene of Tetrahymena thermophila. *Proc. Natl. Acad. Sci. U. S. A.* **83**, 8674–8678 (1986).
13. Piña, B., Martinez, P., Simon, L. & Suau, P. Differential Kinetics of Histone H1.0 Accumulation in Neuronal and Glial Cells from Rat Cerebral Cortex During Postnatal Development. *Biochem. Biophys. Res. Commun.* **123**, 697–702 (1984).
14. Pehrson, J. & Cole, R. D. Histone H10 accumulates in growth-inhibited cultured cells. *Nature* **285**, 43–44 (1980).
15. Fan, Y., Nikitina, T., Morin-Kensicki, E., Zhao, J. & Magnuson, T. H1 linker histones are essential for mouse development and affect nucleosome spacing in vivo. *Mol Cell Biol* **23**, (2003).
16. Orrego, M. *et al*. Differential affinity of mammalian histone H1 somatic subtypes for DNA and chromatin. *BMC Biol.* **5**, 1–11 (2007).
17. Medrzycki, M. *et al*. Histone H1.3 suppresses H19 noncoding RNA expression and cell growth of ovarian cancer cells. *Cancer Res.* **74**, 6463–6473 (2014).
18. Sancho, M., Diani, E., Beato, M. & Jordan, A. Depletion of human histone H1 variants uncovers specific roles in gene expression and cell growth. *PLoS Genet.* **4**, (2008).
19. Meergans, T., Albig, W. & Doenecke, D. Varied Expression Patterns of Human H1 Histone Genes in Different Cell Lines. *DNA Cell Biol.* **16**, 1041–1049 (1997).
20. Jacobsen, F. *et al*. Activity of histone H1.2 in infected burn wounds. *J. Antimicrob.*

Chemother. **55**, 735–741 (2005).
21. Konishi, A. *et al*. Involvement of histone H1.2 in apoptosis induced by DNA double-strand breaks. *Cell* **114**, 673–688 (2003).
22. Hechtman, J. F. *et al*. Promyelocytic leukemia zinc finger and histone H1.5 differentially stain low- and high-grade pulmonary neuroendocrine tumors: A pilot immunohistochemical study. *Hum. Pathol*. **44**, 1400–1405 (2013).
23. Khachaturov, V., Xiao, G. Q., Kinoshita, Y., Unger, P. D. & Burstein, D. E. Histone H1.5, a novel prostatic cancer marker: An immunohistochemical study. *Hum. Pathol*. **45**, 2115–2119 (2014).
24. Talasz, H., Helliger, W., Puschendorf, B. & Lindner, H. In vivo phosphorylation of histone H1 variants during the cell cycle. *Biochemistry* **35**, 1761–1767 (1996).
25. Th'ng, J. P. H., Guo, X. W., Swank, R. A., Crissman, H. A. & Bradbury, E. M. Inhibition of histone phosphorylation by staurosporine leads to chromosome decondensation. *J. Biol. Chem*. **269**, 9568–9573 (1994).
26. Wiśniewski, J. R., Zougman, A., Krüger, S. & Mann, M. Mass spectrometric mapping of linker histone H1 variants reveals multiple acetylations, methylations, and phosphorylation as well as differences between cell culture and tissue. *Mol. Cell. Proteomics* **6**, 72–87 (2007).
27. Tweedie-Cullen, R. Y., Reck, J. M. & Mansuy, I. M. Comprehensive mapping of post-translational modifications on synaptic, nuclear, and histone proteins in the adult mouse brain. *J. Proteome Res*. **8**, 4966–4982 (2009).
28. Meehan, R., Lewis, J. D. & Bird, A. P. Characterization of MECP2, a vertebrate DNA binding protein with affinity for methylated DNA. *Nucleic Acids Res*. **20**, 5085–5092 (1992).
29. Dunker, A. K. *et al*. Intrinsically disordered protein. *J. Mol. Graph. Model*. **19**, 26–59 (2001).
30. Ghosh, R. P., Horowitz-Scherer, R. A., Nikitina, T., Shlyakhtenko, L. S. & Woodcock, C. L. MeCP2 Binds Cooperatively to Its Substrate and Competes with Histone H1 for Chromatin Binding Sites. *Mol. Cell. Biol*. **30**, 4656–4670 (2010).
31. Ghosh, R. P. *et al*. Unique physical properties and interactions of the domains of methylated DNA binding protein 2. *Biochemistry* **49**, 4395–4410 (2010).
32. Chahrour, M. *et al*. MeCP2, a key contributor to neurological disease, activates and represses transcription. *Science (80-.).* **320**, 1224–1229 (2008).
33. Jeffery, L. & Nakielny, S. Components of the DNA methylation system of chromatin control are RNA-binding proteins. *J. Biol. Chem*. **279**, 49479–49487 (2004).
34. Shahbazian, M. D., Antalffy, B., Armstrong, D. L. & Zoghbi, H. Y. Insight into Rett syndrome: MeCP2 levels display tissue- and cell-specific differences and correlate with neuronal maturation. *Hum. Mol. Genet*. **11**, 115–124 (2002).
35. Balmer, D., Goldstine, J., Rao, Y. M. & LaSalle, J. M. Elevated methyl-CpG-binding protein 2 expression is acquired during postnatal human brain development and is correlated with alternative polyadenylation. *J. Mol. Med*. **81**, 61–68 (2003).
36. Amir, R. E. *et al*. Rett syndrome is caused by mutations in X-linked MECP2, encoding methyl- CpG-binding protein 2. *Nat. Genet*. **23**, 185–188 (1999).
37. Neul, J. L. *et al*. Rett syndrome: Revised diagnostic criteria and nomenclature. *Ann. Neurol*. **68**, 944–950 (2010).
38. Kishi, N. & Macklis, J. D. MECP2 is progressively expressed in post-migratory neurons

and is involved in neuronal maturation rather than cell fate decisions. *Mol. Cell. Neurosci.* **27**, 306–321 (2004).
39. Nakashima, H. *et al*. MeCP2 controls neural stem cell fate specification through miR-199a-mediated inhibition of BMP-Smad signaling. *Cell Rep.* **35**, 109124 (2021).
40. Singleton, M. K. *et al*. MeCP2 is required for global heterochromatic and nucleolar changes during activity-dependent neuronal maturation. *Neurobiol. Dis.* **43**, 190–200 (2011).
41. Peters, S. U. *et al*. The behavioral phenotype in MECP2 duplication syndrome: A comparison with idiopathic autism. *Autism Res.* **6**, 42–50 (2013).
42. Matrisciano, F. *et al*. Epigenetic modifications of GABAergic interneurons are associated with the schizophrenia-like phenotype induced by prenatal stress in mice. *Neuropharmacology* **68**, 184–194 (2013).
43. Roux, J. C. *et al*. Modification of Mecp2 dosage alters axonal transport through the Huntingtin/Hap1 pathway. *Neurobiol. Dis.* **45**, 786–795 (2012).
44. Gantz, S. C., Ford, C. P., Neve, K. A. & Williams, J. T. Loss of Mecp2 in substantia nigra dopamine neurons compromises the nigrostriatal pathway. *J. Neurosci.* **31**, 12629–12637 (2011).
45. Hutchinson, A. N., Deng, J. V., Cohen, S. & West, A. E. Phosphorylation of MeCP2 at Ser421 contributes to chronic antidepressant action. *J. Neurosci.* **32**, 14355–14363 (2012).
46. Repunte-Canonigo, V. *et al*. MeCP2 regulates ethanol sensitivity and intake. *Addict. Biol.* **19**, 791–799 (2014).
47. Chen, R. Z., Akbarian, S., Tudor, M. & Jaenisch, R. Deficiency of methyl-CpG binding protein-2 in CNS neurons results in a Rett-like phenotype in mice. *Nat. Genet.* **27**, 327–331 (2001).
48. Guy, J., Hendrich, B., Holmes, M., Martin, J. E. & Bird, A. A mouse Mecp2-null mutation causes neurological symptoms that mimic rett syndrome. *Nat. Genet.* **27**, 322–326 (2001).
49. Jaeger, A. W. & Kuenzle, C. C. The chromatin repeat length of brain cortex and cerebellar neurons changes concomitant with terminal differentiation. *EMBO J.* **1**, 811–816 (1982).
50. Cestelli, A., Castiglia, D., Di Liegro, C. & Di Liegro, I. Qualitative differences in nuclear proteins correlate with neuronal terminal differentiation. *Cell. Mol. Neurobiol.* **12**, 33–43 (1992).
51. Pearson, E. C., Bates, D. L., Prospero, T. D. & Thomas, J. O. Neuronal nuclei and glial nuclei from mammalian cerebral cortex: Nucleosome repeat lengths, DNA contents and H1 contents. *Eur. J. Biochem.* **144**, 353–360 (1984).
52. Lister, R. *et al*. Global epigenomic reconfiguration during mammalian brain development. *Science (80-.).* **341**, (2013).
53. Skene, P. J. *et al*. Neuronal MeCP2 Is Expressed at Near Histone-Octamer Levels and Globally Alters the Chromatin State. *Mol. Cell* **37**, 457–468 (2010).
54. Nan, X., Campoy, F. J. & Bird, A. MeCP2 is a transcriptional repressor with abundant binding sites in genomic chromatin. *Cell* **88**, 471–481 (1997).
55. Ito-Ishida, A. *et al*. Genome-wide distribution of linker histone H1.0 is independent of MeCP2. *Nat. Neurosci.* **21**, 794–798 (2018).
56. Stuss, D. P. *et al*. Impaired in vivo binding of MeCP2 to chromatin in the absence of its DNA methyl-binding domain. *Nucleic Acids Res.* **41**, 4888–4900 (2013).
57. Yazdani, M. *et al*. Disease Modeling Using Embryonic Stem Cells: MeCP2 Regulates Nuclear Size and RNA Synthesis in Neurons. 2128–2139 (2012). doi:10.1002/June

58. Shen, X., Yu, L., Weir, J. W. & Gorovsky, M. A. Linker histories are not essential and affect chromatin condensation in vivo. *Cell* **82**, 47–56 (1995).
59. Deolal, P. & Mishra, K. Regulation of diverse nuclear shapes: pathways working independently, together. *Commun. Integr. Biol.* **14**, 158–175 (2021).
60. Mahajani, S. *et al.* Lamin B1 levels modulate differentiation into neurons during embryonic corticogenesis. *Sci. Rep.* **7**, 1–11 (2017).
61. Belton, J. M. *et al.* Hi-C: A comprehensive technique to capture the conformation of genomes. *Methods* **58**, 268–276 (2012).
62. Boltsis, I., Grosveld, F., Giraud, G. & Kolovos, P. Chromatin Conformation in Development and Disease. *Front. Cell Dev. Biol.* **9**, (2021).
63. Serna-Pujol, N. *et al.* Coordinated changes in gene expression, H1 variant distribution and genome 3D conformation in response to H1 depletion. *Nucleic Acids Res.* **50**, (2022).
64. Bolzer, A. *et al.* Three-dimensional maps of all chromosomes in human male fibroblast nuclei and prometaphase rosettes. *PLoS Biol.* **3**, 0826–0842 (2005).
65. Fraser, J. *et al.* Hierarchical folding and reorganization of chromosomes are linked to transcriptional changes in cellular differentiation. *Mol. Syst. Biol.* **11**, 852 (2015).
66. Meshorer, E. *et al.* Hyperdynamic plasticity of chromatin proteins in pluripotent embryonic stem cells. *Dev. Cell* **10**, 105–116 (2006).
67. Song, Y. *et al.* Data descriptor: A dynamic view of the proteomic landscape during differentiation of rencell VM cells, an immortalized human neural progenitor line. *Sci. Data* **6**, 1–17 (2019).
68. Ito-Ishida, A. *et al.* Genome-wide distribution of linker histone H1.0 is independent of MeCP2. *Nat. Neurosci.* **21**, 794–798 (2018).
69. Riedmann, C. & Fondufe-Mittendorf, Y. N. Comparative analysis of linker histone H1, MeCP2, and HMGD1 on nucleosome stability and target site accessibility. *Sci. Rep.* **6**, 1–11 (2016).
70. Jung, B. P. *et al.* The expression of methyl CpG binding factor MeCP2 correlates with cellular differentiation in the developing rat brain and in cultured cells. *J. Neurobiol.* **55**, 86–96 (2003).
71. Olson, C. O., Zachariah, R. M., Ezeonwuka, C. D., Liyanage, V. R. B. & Rastegar, M. Brain region-specific expression of MeCP2 isoforms correlates with DNA methylation within Mecp2 regulatory elements. *PLoS One* **9**, (2014).
72. Piña, B., Martínez, P. & Suau, P. Changes in H1 complement in differentiating rat-brain cortical neurons. *Eur. J. Biochem.* **164**, 71–76 (1987).
73. Martínez De Paz, A. *et al.* MeCP2-E1 isoform is a dynamically expressed, weakly DNA-bound protein with different protein and DNA interactions compared to MeCP2-E2. *Epigenetics and Chromatin* **12**, 1–16 (2019).
74. Perez-castillo, A., Bernal, J., Ferreiro, B. & Pans, T. The early ontogenesis of thyroid hormone receptor in the rat fetus. *Endocrinology* **117**, 2457–2461 (1985).
75. Dominguez, V., Pina, B. & Suau, P. Histone H1 subtype synthesis in neurons and neuroblasts. *Development* **115**, 181–185 (1992).
76. Hoffrogge, R. *et al.* 2-DE proteome analysis of a proliferating and differentiating human neuronal stem cell line (ReNcell VM). *Proteomics* **6**, 1833–1847 (2006).
77. Tsujimura, K., Abematsu, M., Kohyama, J., Namihira, M. & Nakashima, K. Neuronal differentiation of neural precursor cells is promoted by the methyl-CpG-binding protein MeCP2. *Exp. Neurol.* **219**, 104–111 (2009).

78. Medrzycki, M., Zhang, Y., Cao, K. & Fan, Y. Expression analysis of mammalian linker-histone subtypes. *J. Vis. Exp.* (2012). doi:10.3791/3577
79. Smith, B. J., Walker, J. M. & Johns, E. W. Structural Homology Between A Mammalian H1.0 Subfraction and Avian Erythrocyte-specific Histone H5. **112**, 42–44 (1980).
80. Shay, C. E., Foster, P. G. & Neelin, J. M. Immunological relationships among vertebrate lysine-rich histones. *Comp. Biochem. Physiol.* **91**, 69–78 (1988).
81. Boix, J. & Ruiz-Carrillo, A. Increased histone H1 ° expression in differentiating mouse erythroleukemia cells is related to decreased cell proliferation. *Exp. Cell Res.* **201**, 531–534 (1992).
82. Maezawa, I., Swanberg, S., Harvey, D., LaSalle, J. M. & Jin, L. W. Rett syndrome astrocytes are abnormal and spread MeCP2 deficiency through gap junctions. *J. Neurosci.* **29**, 5051–5061 (2009).
83. Ponte, I. *et al*. Transcriptional activation of Histone H1° during neuronal terminal differentiation. *Dev. Brain Res.* **80**, 35–44 (1994).
84. Sirotkin, A., Edelmann, W., Cheng, G., Klein-Szanto, A. & Kucherlapati, R. Mice develop normally without the H1(0) linker histone. *Proc. Natl. Acad. Sci. U. S. A.* **92**, (1995).
85. Fan, Y., Sirotkin, A., Russell, R. G., Ayala, J. & Skoultchi, A. I. Individual Somatic H1 Subtypes Are Dispensable for Mouse Development Even in Mice Lacking the H1 0 Replacement Subtype . *Mol. Cell. Biol.* **21**, 7933–7943 (2001).
86. Urdinguio, R. G. *et al*. Mecp2-null mice provide new neuronal targets for rett syndrome. *PLoS One* **3**, (2008).
87. Sollberger, G. *et al*. Linker histone h1.2 and h1.4 affect the neutrophil lineage determination. *Elife* **9**, 1–24 (2020).
88. Armstrong, D., Dunn, J. K., Antalffy, B. & Trivedi, R. Selective Dendritic Alterations in the Cortex of Rett Syndrome. *J. Neuropathol. Exp. Neurol.* **54**, 195–201 (1995).
89. Dixon, J. R. *et al*. Topological domains in mammalian genomes identified by analysis of chromatin interactions. *Nature* **485**, 376–380 (2012).
90. de la Torre-Ubieta, L. *et al*. The Dynamic Landscape of Open Chromatin during Human Cortical Neurogenesis. *Cell* **172**, 289-304.e18 (2018).
91. Li, Y. *et al*. Global transcriptional and translational repression in human-embryonic- stem-cell-derived rett syndrome neurons. *Cell Stem Cell* **13**, 446–458 (2013).
92. Rietveld, L., Stuss, D. P., McPhee, D. & Delaney, K. R. Genotype-specific effects of Mecp2 loss-of-function on morphology of layer V pyramidal neurons in heterozygous female Rett syndrome model mice. *Front. Cell. Neurosci.* **9**, 1–17 (2015).
93. Kalukula, Y., Stephens, A. D., Lammerding, J. & Gabriele, S. Mechanics and functional consequences of nuclear deformations. **0123456789**,
94. D'Anna, J. A. & Tobey, R. A. Changes in Histone HI Content and Chromatin Structure of Cells Blocked in Early S Phase by 5-Fluorodeoxyundine and Aphidicolin. *Biochemistry* **23**, 5024–5029 (1984).
95. Happel, N., Warneboldt, J., Hänecke, K., Haller, F. & Doenecke, D. H1 subtype expression during cell proliferation and growth arrest. *Cell Cycle* **8**, 2226–2232 (2009).
96. Hirofuji, S. *et al*. Mitochondrial dysfunction in dopaminergic neurons differentiated from exfoliated deciduous tooth-derived pulp stem cells of a child with Rett syndrome. *Biochem. Biophys. Res. Commun.* **498**, 898–904 (2018).
97. Samaco, R. C. *et al*. Loss of MeCP2 in aminergic neurons causes cell-autonomous defects

in neurotransmitter synthesis and specific behavioral abnormalities. *Proc. Natl. Acad. Sci.* **106**, 21966–21971 (2009).
98. Shah, R. R. *et al*. Efficient and versatile CRISPR engineering of human neurons in culture to model neurological disorders. *Wellcome Open Res*. **1**, 1–21 (2016).
99. Ballas, N., Lioy, D. T., Grunseich, C. & Mandel, G. Non-cell autonomous influence of MeCP2-deficient glia on neuronal dendritic morphology. *Nat. Neurosci*. **12**, 311–317 (2009).
100. Williams, E. C. *et al*. Mutant astrocytes differentiated from Rett syndrome patients-specific iPSCs have adverse effects on wildtype neurons. *Hum. Mol. Genet*. **23**, 2968–2980 (2014).
101. Tyssowski, K., Kishi, Y. & Gotoh, Y. Chromatin regulators of neural development. *Neuroscience* **264**, 4–16 (2014).
102. Zlatanova, J. & Van Holde, K. Linker histones versus HMG 1/2: A struggle for dominance? *BioEssays* **20**, 584–588 (1998).
103. Catez, F., Brown, D. T., Misteli, T. & Bustin, M. Competition between histone H1 and HMGN proteins for chromatin binding sites. *EMBO Rep*. **3**, 760–766 (2002).
104. Schneider, R. *et al*. Histone H3 lysine 4 methylation patterns in higher eukaryotic genes. *Nat. Cell Biol*. **6**, 73–77 (2004).
105. Jenuwein, T. & Allis, C. D. Translating the Histone Code. **293**, 1074–1080 (2001).
106. Strahl, B. D. & Allis, C. D. The language of covalent histone modifications. *Nature* **403**, 41–45 (2000).
107. Kamieniarz, K. *et al*. A dual role of linker histone H1.4 Lys 34 acetylation in transcriptional activation. 797–802 (2012). doi:10.1101/gad.182014.111.GENES
108. Ausio, J., Borochov, N., Seger, D. & Eisenberg, H. Interaction of chromatin with NaCl and MgCl2. Solubility and binding studies, transition to and characterization of the higher-order structure. *J. Mol. Biol*. **177**, 373–398 (1984).
109. Laemmli, U. K. Cleavage of Structural Proteins during the Assembly of the Head of Bacteriophage T4. *Nature* **227**, 680–685 (1970).
110. Medrzycki, M., Zhang, Y., McDonald, J. F. & Fan, Y. Profiling of linker histone variants in ovarian cancer. *Front Biosci* **17**, 396–406 (2013).
111. Geigges, M. *et al*. Reference Genes for Expression Studies in Human CD8+ Naïve and Effector Memory T Cells under Resting and Activating Conditions. *Sci. Rep*. **10**, 1–12 (2020).

Appendices

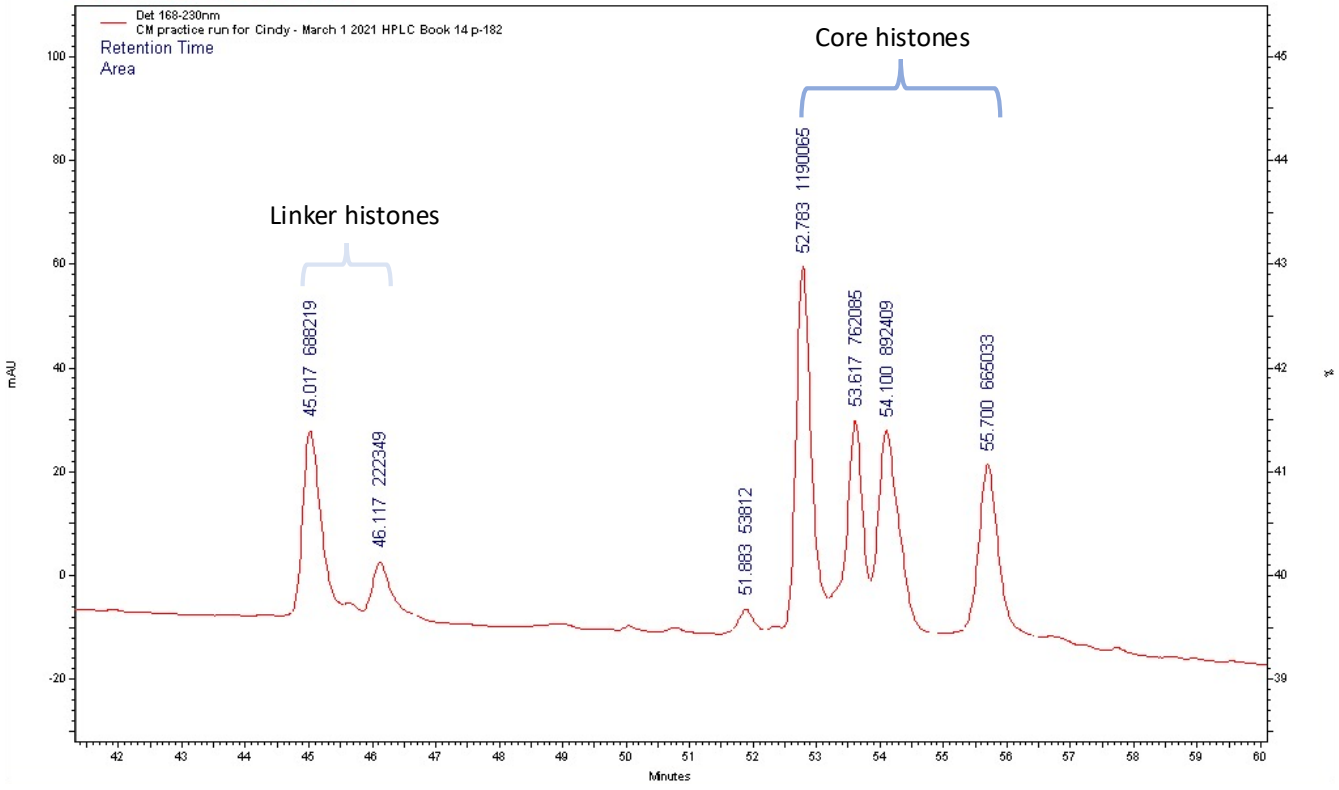

Retention Time	Area	
45.017	688219	Total area of linker histone peaks: 910568
46.117	222349	
51.883	53812	
52.783	1190065	Total area of core histone peaks: 3509592
53.617	762085	
54.1	892409	
55.7	665033	

Linker histone to core histone ratio =

$$\frac{\textit{Total area of linker histone peaks}}{\textit{Total area of core histone peaks}}$$

$$= \frac{910568}{3509592} = 0.26$$

Appendix A. Sample calculation of linker to core histone ratio using the HPLC chromatogram data for CM.

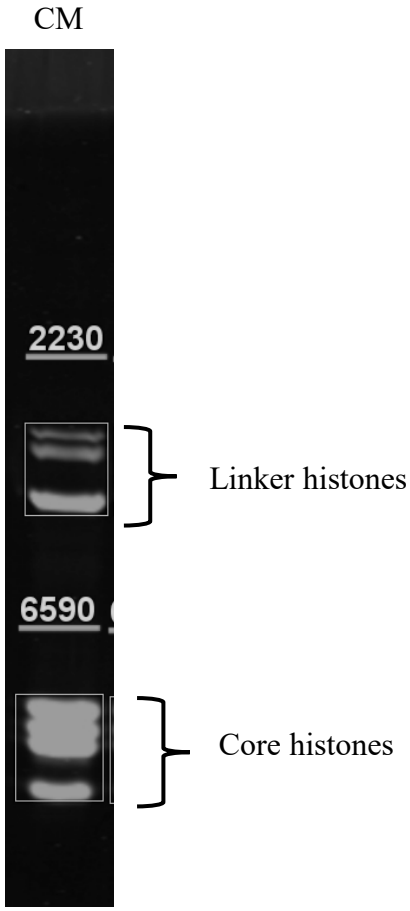

Linker histone/core histone of chicken erythrocytes (CM)

$$\frac{linker\ histone}{core\ histone} = \frac{2230}{6590} = \mathbf{0.34}$$

Appendix B. Quantification of Coomassie-stained protein bands on SDS-PAGE and sample calculation of linker histone/core histone ratio using densitometrically obtained values. Gel was imaged and bands were quantified using Li-Cor Odyssey Clx (LI-COR Biosciences, Lincoln, NE, USA).

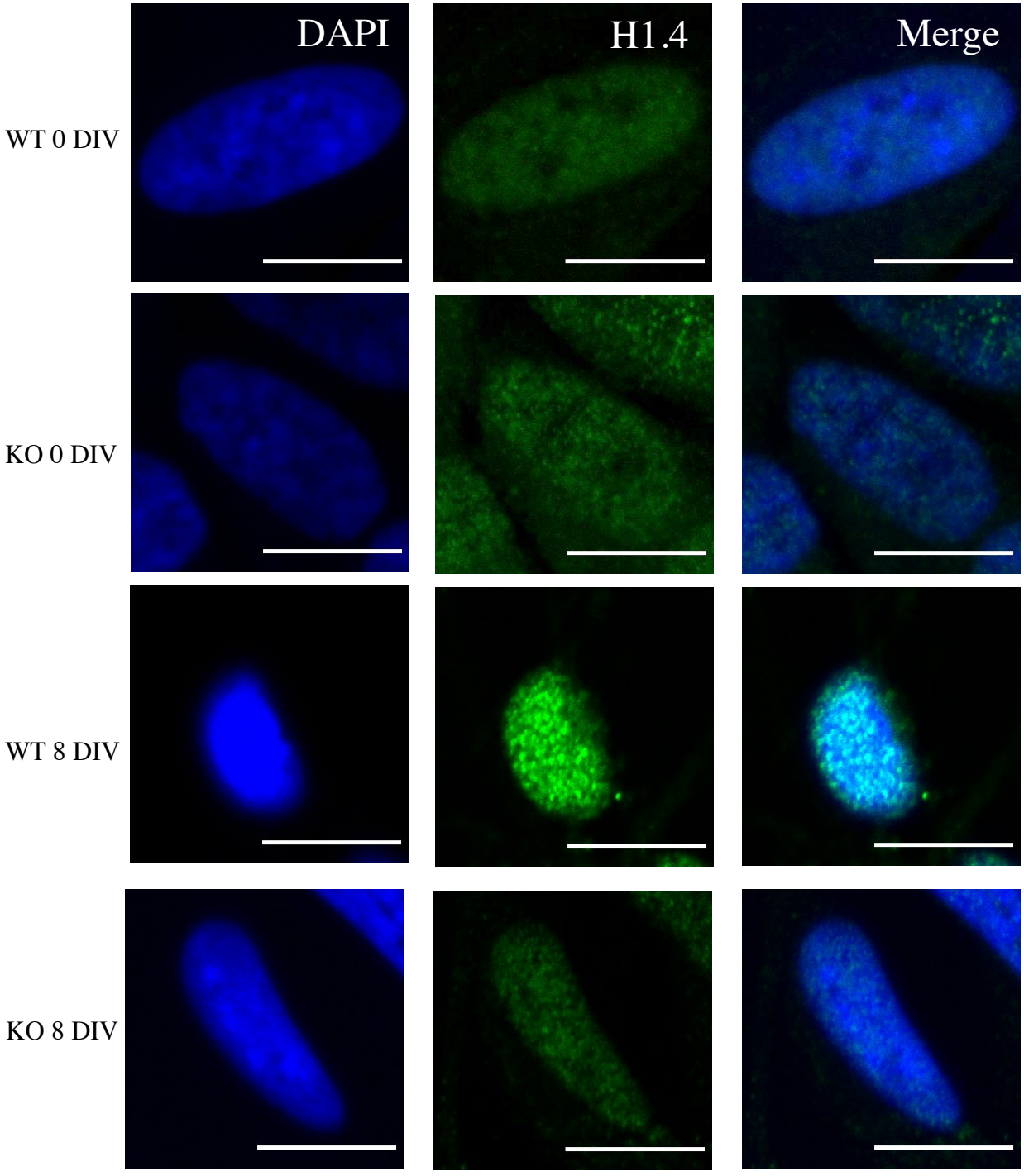

Appendix C. Set #2 of close-up images of ReNCell WT and KO at 0 and 8 DIV (set #1 is shown in Figure 2. 22). Cells were imaged with DAPI (blue), H1.4 antibody (green). These are close-up images of one nucleus found in the images shown in Figure 2. 21. Scale bars represent 10 μm.

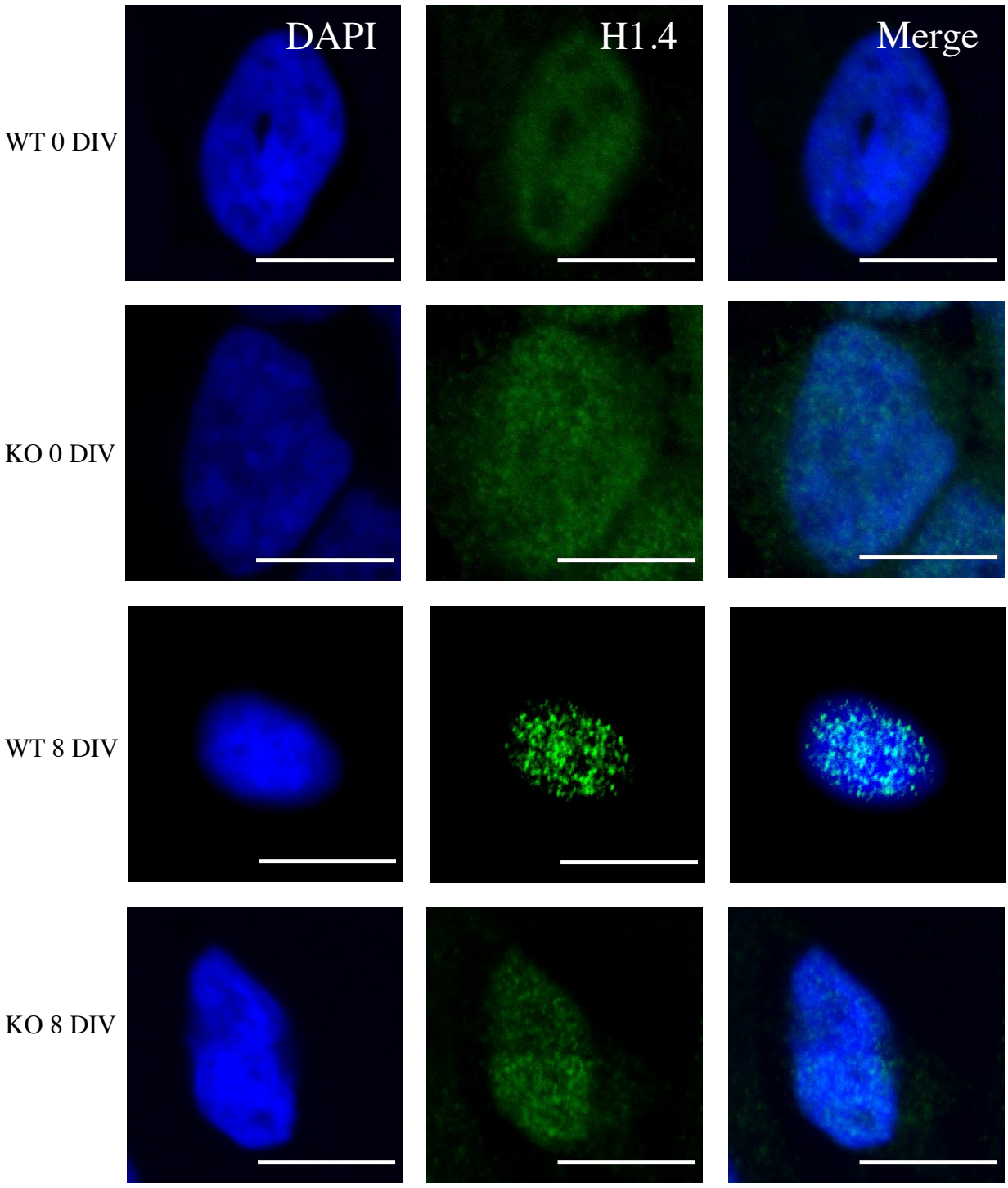

Appendix D. Set #3 of close-up images of ReNCell WT and KO at 0 and 8 DIV (set #1 is shown in Figure 2. 22). Cells were imaged with DAPI (blue), H1.4 antibody (green). These are close-up images of one nucleus found in the images shown in Figure 2. 21. Scale bars represent 10 μm.

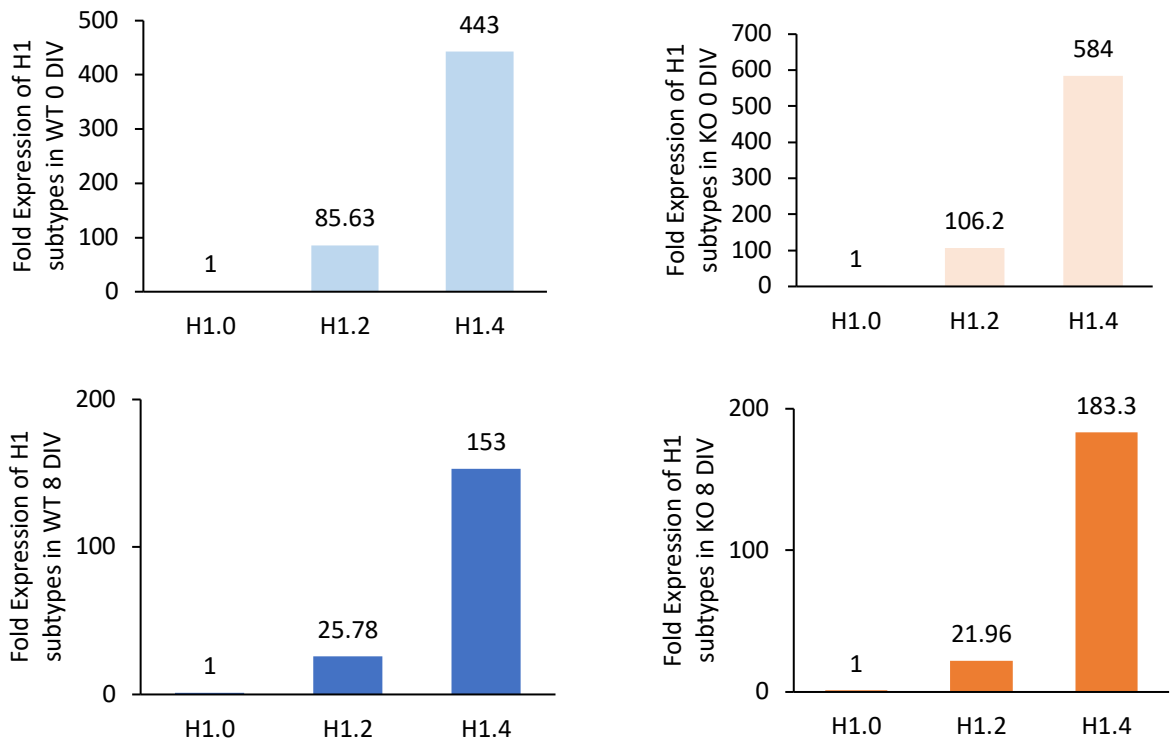

Appendix E. Relative fold expression of histone H1 subtypes in WT and KO ReNCell at 0 and 8 DIV. The fold expression levels shown are relative to that of H1.0 in each sample.